https://doi.org/10.5194/egusphere-2024-2416
Preprint. Discussion started: 20 August 2024

Measurement Report: Optical and structural properties of atmospheric water-soluble organic carbon in China: Insights from multi-site spectroscopic measurements

Haibiao Chen[1,2], Caiqing Yan[1], Liubin Huang[1], Lin Du[1,3], Yang Yue[3], Xinfeng Wang[1], Qingcai Chen[4], Mingjie Xie[2], Junwen Liu[5], Fengwen Wang[6], Shuhong Fang[7], Qiaoyun Yang[8], Hongya Niu[9], Mei Zheng[10], Yan Wu[3], Likun Xue[1]

[1]Qingdao Key Laboratory for Prevention and Control of Atmospheric Pollution in Coastal Cities, Environment Research Institute, Shandong University, Qingdao, 266237, China
[2]Collaborative Innovation Center of Atmospheric Environment and Equipment Technology, Jiangsu Key Laboratory of Atmospheric Environment Monitoring and Pollution Control (AEMPC), Nanjing University of Information Science & Technology, Nanjing, 210044, China
[3]School of Environmental Science and Engineering, Shandong University, Qingdao, 266237, China
[4]School of Environmental Science and Engineering, Shaanxi University of Science and Technology, Xi'an, 710021, China
[5]Institute for Environmental and Climate Research, Jinan University, Guangzhou, 511443, China
[6]State Key Laboratory of Coal Mine Disaster Dynamics and Control, Department of Environmental Science, Chongqing University, Chongqing, 400030, China
[7]College of Resources and Environment, Chengdu University of Information Technology, Chengdu, 610225, China
[8]Department of Occupational and Environmental Health, School of Public Health, Tianjin Medical University, Tianjin, 300070, China
[9]Key Laboratory of Resource Exploration Research of Hebei Province, Hebei University of Engineering, Handan, 056038, China
[10]SKL-ESPC, College of Environmental Sciences and Engineering, and Center for Environment and Health, Peking University, Beijing, 100871, China

Correspondence to: Caiqing Yan (cyan0325@sdu.edu.cn)

Abstract. To understand the spatial variation of optical and structural properties of water-soluble brown carbon and its influencing factors in China, the light absorption, fluorescence, and Fourier transform infrared (FTIR) spectrum of water-soluble organic carbon (WSOC) in different regions of China are measured following the same analytical methods. The average light absorption coefficients and mass absorption efficiencies of WSOC at 365 nm (Abs_{365} and MAE_{365}) rank from high to low as northwest China > southwest China > north China > east China > regional site, with higher values in Northern China than Southern China and regional sites, and higher values in inland areas than coastal areas. The light absorption factors resolved by positive matrix factorization model combined with light absorption spectra and abundant aromatic O-H and C=C functional groups determined by FTIR both indicate that aromatic compounds are important light-absorbing substances in WSOC, which also have a significant impact on fluorophores. Multiple linear regression analysis shows that the identified fluorophores by fluorescence spectra combined with parallel factor analysis contribute to about 62-93% of the WSOC light absorption at all sites, in which humic-like substance (HULIS) contributes the most, especially highly-oxygenated HULIS (29%-50%) with long emission wavelengths. Combustion source emissions and atmospheric chemical processes have significant impacts on

https://doi.org/10.5194/egusphere-2024-2416
Preprint. Discussion started: 20 August 2024

the WSOC light absorption at some sites. Moreover, relative humidity (RH) can also affect MAE_{365} of WSOC with MAE_{365} values decreasing with the increase of RH when RH < 60% and remaining relatively unchanged when RH > 60%. Taken together, this study promotes a better understanding of the spatial heterogeneity of optical and structural properties of WSOC and their influencing factors in China.

1 Introduction

Brown carbon (BrC) is an important type of carbonaceous aerosol that absorbs light over the ultraviolet and visible (UV-Vis) range and exhibits a strong wavelength dependence (Andreae and Gelencsér, 2006). BrC has substantial effects on atmospheric radiative forcing and regional climate due to its strong light absorption ability in the UV-Vis range and has attracted widespread attention in recent years (Laskin et al., 2015). It has been simulated that BrC contributes up to 72% of the total light absorption of aerosols at 370 nm and the direct radiative effect of BrC (+0.048 $W \cdot m^{-2}$) is about 30% of black carbon (+0.17 $W \cdot m^{-2}$) (Wang et al., 2018). However, the lack of field measurements limits the model's ability to extend to global simulations of BrC. The spatiotemporal variation of optical properties of BrC is one of the key factors leading to the uncertainty in the radiation assessment of organic aerosols. A comprehensive and clear understanding of optical properties of BrC in different regions is essential to accurately assess the atmospheric radiative forcing of aerosols.

Absorption and fluorescence spectroscopy are two of the most commonly and widely used methods to reveal optical properties of BrC (Wu et al., 2021; Wang et al., 2022b), and solvent-soluble organic carbon (e.g., water-soluble organic carbon, WSOC) generally act as a substitute of BrC. By light-absorption spectroscopy analysis, light absorption characteristics and capabilities of BrC from different sources or environments are usually characterized by the absorption coefficient or mass absorption efficiency of a specific wavelength, usually choosing 360-370 nm (average 365 nm) (Hecobian et al., 2010). And the direct radiative forcing of water-soluble BrC (WS-BrC) is subsequently evaluated by simplified radiative forcing models with the measured absorption coefficients. By fluorescence spectroscopy method, fluorescence spectra are used to characterize fluorescence fingerprints of source and environmental samples, provide source-related information according to fluorescent indices, identify chromophores in BrC with a combination of parallel factor analysis (PARAFAC), and infer the chemical and structural characteristics of BrC chromophores (Wu et al., 2021; Chen et al., 2020).

Based on spectroscopic methods, studies conducted in different countries or regions all over the world show that there are significant spatiotemporal differences in the light absorption characteristics of BrC. For example, the mass absorption efficiency of WS-BrC is generally higher in Asia than in North America and Europe, and higher in winter compared to summer (Hecobian et al., 2010; Wang et al., 2022a; Kirillova et al., 2014; Teich et al., 2017). Furthermore, light absorption of BrC can also vary from location to location even within the same region (Cao et al., 2024). However, the current understanding of spatial differences in light absorption and fluorescence characteristics of BrC is mainly based on the results from different laboratories with different extraction and analysis methods. This may affect the interpretation and accuracy of comparison results due to differences in the analysis methods. For example, it has been shown that the size of the syringe filter could lead

https://doi.org/10.5194/egusphere-2024-2416
Preprint. Discussion started: 20 August 2024

to differences in the solvent-soluble BrC light absorption measurement results (Zhang et al., 2022a). Therefore, it will be more convincing and necessary to use a uniform method to compare the optical properties of BrC in different regions.

Previous studies have suggested that there may be a link between the light absorption and fluorescence components of BrC (Niu et al., 2022; Tang et al., 2021; Chen et al., 2019), as the necessary condition for an organic compound to produce a fluorescent signal is that it absorbs light. This means that fluorescent substances must be able to absorb light, and substances that can absorb light are not necessarily fluorescent. However, studies on the relationship between light absorption and fluorescence of BrC are still very limited, and the contribution of fluorescent components identified by the commonly used three-dimensional fluorescence spectroscopy to the light absorption of BrC has not been well quantified. Additionally, Fourier transform infrared (FTIR) has been used for the structural characterization of BrC as a non-destructive spectral analysis method that can provide the functional group structure information of compounds (Dey and Sarkar, 2024). The addition of FTIR spectroscopy analysis helps to better understand the structural features that affect the optical properties of BrC. However, different spectral methods are often used separately in previous studies, so the optical and structural characteristics of BrC could not be fully predicted.

In this study, $PM_{2.5}$ is collected from ten sites in different regions of China, and the mass concentration, light absorption and fluorescent spectra, and functional group structures of WSOC are analyzed using a unified method, aiming to explore the spatial heterogeneity of optical properties of WS-BrC in different regions of China and its influencing factors, reveal the relationship between light absorption, fluorescence and functional group structure of WS-BrC, and quantify the contribution of fluorescent chromophores to the light absorption of WS-BrC based on the multi-sites and different spectral dataset.

2 Material and methods

2.1 Ambient $PM_{2.5}$ sample collection

$PM_{2.5}$ samples are collected at eight urban sites and two regional sites in China during the wintertime of 2019-2020 (see Figure 1). The eight cities are distributed in different administrative regions of China, including Tianjin (TJ) and Handan (HD) in north China, Qingdao (QD), Nanjing (NJ) and Shanghai (SH) in east China, Xi'an (XA) in northwest China, Chengdu (CD) and Chongqing (CQ) in southwest China. These cities are representative of their respective regional economies and cultures, with discrepancies in energy structure, geographical and climatic characteristics. The two regional sites locate in Mt. Tai (TS) and Heshan (HS), respectively. TS (1534 m a.s.l.) locates in the middle of the North China Plain, which is less affected by anthropogenic emissions and could better represent the background atmosphere characteristics in Northern China (Jiang et al., 2020). The HS site is located at the Atmospheric Super Monitoring Station in Guangdong, China and downwind of the Pearl River Delta (PRD), which is mainly surrounded by farmland protection areas and forest land with no obvious industrial or urban traffic pollution sources in the vicinity, and can act as a representative regional receptor site for the PRD region. More detailed sampling information is summarized in Table S1. Before sampling, all quartz filters used for sample collection are prebaked at 550 °C for 5.5 h to remove potential organic matter. After sampling, all samples are wrapped in prebaked aluminum

https://doi.org/10.5194/egusphere-2024-2416
Preprint. Discussion started: 20 August 2024

foils and stored in the refrigerator under -20 °C until further analysis.

2.2 Carbonaceous components mass concentration measurement

The measurement of carbonaceous component concentrations can be referred to our previous study (Chen et al., 2023). Briefly, organic carbon (OC) and elemental carbon (EC) are analyzed using a thermal optical transmittance (TOT) carbon analyzer (Sunset Laboratory, Inc., Tigard, OR, USA) with the National Institute for Occupational Safety and Health (NIOSH) protocol. A series of sucrose standard solutions are applied to ensure the status of the instrument and calibrate the final OC and EC concentrations. Concentrations of primary organic carbon (POC) and secondary organic carbon (SOC) are estimated according to the EC-tracer method and more details can be found in Text S1. A portion of each filter (about 6 cm^2) is extracted with ultrapure water (>18.2 MΩ·cm, 25 °C, Direct-Q, Millipore) by ultra-sonication for 30 min, and then the extract is filtered through a 0.45 μm PTFE pore syringe filter (Pall, USA) to remove water-insoluble materials. WSOC concentrations are analyzed using a total organic carbon (TOC) analyzer (Elementar, Germany) and a series of concentration gradient potassium hydrogen phthalate ($C_8H_5O_4K$) standard solutions are used for calibration and correction. Each sample is analyzed in triplicate, and the average of two adjacent values is recorded to minimize error.

2.3 WSOC light absorption spectra measurement and light absorption factor determination

The light-absorbing spectra of WSOC are measured using a spectrophotometer (TIDAS®S 300 UV/VIS 1972 DH, J&M, Germany) coupled with a 1 m path-length liquid waveguide capillary cell (LWCC-3100, World Precision Instruments Inc., USA) over the wavelength range of 250-700 nm with 1 nm scanning interval. Ultrapure water is used as the blank reference during the light absorption spectrum measurement. Light absorption parameters such as light absorption coefficients at 365 nm (Abs_{365}), mass absorption efficiency at 365 nm and 405 nm (MAE_{365} and MAE_{405}), Ångström exponent over 330-400 nm ($AAE_{330\text{-}400}$), and imaginary part (k) of the particle refractive index are calculated and more details can be found in Text S2. Furthermore, the direct radiative effect of water-soluble BrC is calculated by a simplified radiative forcing model with the measured absorption coefficients in this study following the method described in Text S3. To further analyze the light-absorbing properties of WSOC and compare the discrepancies between different sites, a method based on positive matrix factorization (PMF, EPA PMF 5.0) model combined with light absorption spectra (PMF-LAS) is introduced to analyze the light absorption factor in the main light absorption bands of BrC (250-400 nm, interval 5 nm). More details about the PMF-LAS method can be found in Text S4.

2.4 Fluorescent spectra measurement and fluorescence factors determination

The excitation-emission matrix spectra (EEMs) of WSOC are recorded by a fluorescence spectrometer (Duetta™, Horiba Scientific, Japan) in the excitation wavelength (Ex) and emission wavelength (Em) range of 250-600 nm with 5 nm slit width. The intervals of the Ex and Em are 5 nm and 2 nm (4 pixels), respectively. Similarly, ultrapure water is used as the blank reference during the fluorescence spectrum measurement. Fluorescence parameters such as fluorescence index (FI), biological

https://doi.org/10.5194/egusphere-2024-2416
Preprint. Discussion started: 20 August 2024

index (BIX) and humidification index (HIX) are calculated according to the method described in our previous study (Chen et al., 2024) and descriptions in Text S5. And fluorescent components of WSOC are determined based on the PARAFAC model (Chen et al., 2024).

2.5 FTIR spectra analysis

To determine the functional groups in WSOC, an FTIR spectrometer (Nicolet iS50, Thermo Scientific, USA) is employed to obtain the infrared spectrum of WSOC. Briefly, a portion of the filtered extract is freeze-dried and the dried powder is placed on the diamond window of the Attenuated Total Reflection (ATR) platform for measurement. The spectrum is recorded in the average of 128 scans with the wavenumber range of 4000-550 cm^{-1} at a resolution of 4 cm^{-1}. The background spectrum is collected every 60 minutes. It is worth mentioning that the field blank sample is not measured due to almost no powder in the extract of the blank sample after freeze-drying. The baseline correction and smooth processing of the original spectrum are performed through the OMNIC software (v 9.2), and each functional group is integrated using this software. Relative quantitative of functional groups is achieved by calculating the proportion of each peak area to the total peak area.

2.6 Relationship and influencing factor analysis

Multiple linear regression (MLR) model is applied to reveal the relationship between fluorophores and WSOC light absorption and to quantify the contribution of fluorophores to light absorption. To evaluate the contribution of different fluorophores to the light absorption coefficient, ridge regression in MLR model is used to analyze the relationship between the fluorescence intensities of fluorophores and Abs_{365}. In the model calculation process, the Abs_{365} is treated as the dependent variable and the maximum fluorescence intensity is introduced as the independent variable, and insignificant ($p < 0.05$) fluorescent components are excluded from the regression. The calculation is mainly carried out through SPSS software (IBM SPSS Statistics 23). Besides, the extreme gradient boosting (XGBoost) model is applied to verify the results from MLR (Li et al., 2024). Additionally, the XGBoost model is also used to evaluate the influence of conventional gas parameters (e.g., CO, SO_2, O_3, NO_2) on the light absorption of WSOC. More detailed description about the XGBoost method can be found in Text S6.

3 Results and discussion

3.1 Spatial similarity and heterogeneity of WSOC

3.1.1 Concentration levels of WSOC

During the wintertime observation period, WSOC mass concentrations exhibit a significant spatial variation across the ten sites ($p < 0.05$) (see Figure 1 and Table S2). Overall, the average WSOC concentrations rank from high to low as HD > CQ > XA > CD > NJ > TJ > HS > QD > TS > SH. Meanwhile, the average OC and EC mass concentrations rank in the order of CQ > HD > XA > CD > NJ > TJ > HS > QD > TS > SH and XA > HD > NJ > CQ > CD > HS > QD > TJ > TS > SH, respectively.

https://doi.org/10.5194/egusphere-2024-2416
Preprint. Discussion started: 20 August 2024

The regional average carbonaceous component concentration shows a trend of northwest China > southwest China > north China > east China > regional site, with increasing concentrations of carbonaceous aerosols with $PM_{2.5}$ mass concentrations (see Figure S1). Moreover, concentrations of carbonaceous components in inland cities (i.e., HD, NJ, XA, CD, CQ) are much higher than those in coastal cities (i.e., TJ, QD, SH) ($p < 0.01$), which is consistent with that reported in a previous study (Zhang et al., 2022b). This may be attributed to better atmospheric diffusion conditions in coastal areas that are generally more conducive to aerosol diffusion and dilution. Aerosol mass concentrations are lower when air masses come from the ocean (Diesch et al., 2012). Notably, the mass concentrations of carbonaceous components at TS site are very low, which may be due to its high altitude and minimal impact from direct anthropogenic emissions. However, mass concentrations of carbonaceous components at HS site are not that low, which may be due to its location downwind in the PRD, making it more susceptible to long-distance transport of pollutants emitted by cities in the PRD region. Over the study period, the OC/EC and WSOC/OC ratios, which can characterize primary sources of carbonaceous aerosols and formation of secondary organic aerosols as well as atmospheric oxidation levels (Ram et al., 2012; Wang et al., 2016), vary from 2.69 to 19.53 (4.58-10.05 on average) and 22.7% to 96.1% (53.4%-73.3% on average) across the ten sites, indicating non-negligible impacts from both combustion-related emissions and secondary formation on carbonaceous aerosols.

3.1.2 Light absorption of WSOC

As shown in Figure 1 and Figure S2, the light absorption coefficients and mass absorption efficiency at 365 nm (Abs_{365} and MAE_{365}) of WSOC at ten sites display significant spatial discrepancies (1.12-13.07 Mm^{-1} and 0.56-1.26 $m^2 \cdot g^{-1}$ on average, $p < 0.05$). MAE_{365} in SH, CD, TS and HS (0.56-0.74 $m^2 \cdot g^{-1}$ on average) are comparable to those reported in light polluted areas such as in Guangzhou, Lulang, Waliguan, Urumqi in China and Los Angeles in the USA (0.48-0.81 $m^2 \cdot g^{-1}$) (Fan et al., 2016; Liu et al., 2018; Soleimanian et al., 2020; Wu et al., 2020; Xu et al., 2020; Zhong et al., 2023), while they are all lower than those in TJ, HD, QD, NJ, XA and CQ (0.89-1.26 $m^2 \cdot g^{-1}$ in average), which are comparable to those reported in heavily polluted areas such as in Beijing, Xining, Yinchuan, Lanzhou, Taipei in China and Patiala and Mohanpur in India (0.93-1.30 $m^2 \cdot g^{-1}$) (Cheng et al., 2016; Srinivas et al., 2016; Dey et al., 2021; Zhong et al., 2023; Ting et al., 2022). Generally, the measured Abs_{365} and MAE_{365} at different sites rank as HD > XA > CQ > NJ > CD > TJ > QD > HS > TS > SH and HD > XA > QD > CQ > NJ > TJ > TS > CD > HS > SH, respectively, and the regional average Abs_{365} and MAE_{365} display as northwest China > southwest China > north China > east China > regional site. Moreover, the Abs_{365} and MAE_{365} are higher ($p < 0.01$) in Northern China (including TJ, HD, QD, and XA, 7.34 ± 5.21 Mm^{-1} and 1.02 ± 0.29 $m^2 \cdot g^{-1}$) than in Southern China (including NJ, SH, CD, and CQ, 5.86 ± 3.91 Mm^{-1} and 0.78 ± 0.23 $m^2\ g^{-1}$) and regional sites (e.g., TS and HS, 2.91 ± 1.38 Mm^{-1} and 0.72 ± 0.23 $m^2 \cdot g^{-1}$), and higher ($p < 0.01$) in inland (8.24 ± 4.75 Mm^{-1} and 0.91 ± 0.27 $m^2 \cdot g^{-1}$) than in coastal areas (4.37 ± 3.52 Mm^{-1} and 0.88 ± 0.32 $m^2 \cdot g^{-1}$), which are consistent with the regional differences in carbonaceous component concentrations. The spatial variation may be related to the diversities in the source and composition of WSOC at different sites. For example, the increase in primary emissions such as coal combustion and biomass burning during the winter heating period in Northern China will lead to an enhancement of the WSOC light absorption (Zhang et al., 2021). The strong correlation ($p < 0.01$) between Abs_{365}

https://doi.org/10.5194/egusphere-2024-2416
Preprint. Discussion started: 20 August 2024

and POC (*r* range: 0.59-0.90) or SOC (*r* range: 0.43-0.97) (see Figure S3) indicates that light-absorbing components in WSOC are simultaneously affected by both primary emission and secondary formation.

Figure 2 illustrates the $\log_{10}(MAE_{405})$ and $AAE_{330-400}$ values of WS-BrC measured in this study and reported in previous studies. Notably, most values measured at the ten sites in this study fall in the regions of weakly-absorbing BrC (W-BrC). This is similar to the region where the light absorption parameters of WS-BrC obtained in other studies are located. Although the $\log_{10}(MAE_{405})$ values of WS-BrC in QD are close to that of W-BrC and moderately-absorbing BrC (M-BrC), its higher AAE values do not exactly fall into these categories, but are closer to the value of biomass burning samples, indicating that biomass burning emission has a great influence on the light absorption of wintertime WS-BrC at the site in QD. This may be related to the residential heating activities around the sampling site. In contrast, the wintertime samples in XA are mainly distributed in the M-BrC region, with a few samples in the W-BrC region. This indicates that WS-BrC in XA has stronger light-absorbing ability, which is consistent with its higher Abs_{365} and MAE_{365} values.

Accordingly, the direct radiative forcing within the wavelength range of 300-400 nm ($SFE_{300-400}$) and 300-700 nm ($SFE_{300-700}$) in different regions are calculated based on the measured MAE values, Ångström exponent and mass concentrations. The dSFE/dλ spectra and integrated SFE values are shown in Figure S4. Generally, there exist significant spatial variations in SFE values among different sites. HD (SH) has the highest (lowest) $SFE_{300-400}$ (1.92 ± 0.51 W g^{-1} (0.88 ± 0.17 W·g^{-1})) and $SFE_{300-700}$ values (4.50 ± 1.25 W·g^{-1} (1.82 ± 0.38 W·g^{-1})), which is related to their strong (weak) light-absorbing ability and high (low) mass concentrations of WSOC. It should be noted that $SFE_{300-400}$ accounts for more than 40% (38.6-48.9% on average) of $SFE_{300-700}$ across the ten sites in this study, which is consistent with a previous study (Deng et al., 2022), indicating that the light absorption of WSOC plays a crucial role in the aerosol direct radiative forcing in the UV-Vis range. Notably, there is a significant negative correlation ($p<0.01$) between SFE value and WSOC/OC in most sites (see Figure S4c and d), implying that the radiation effect of aerosols may decrease as the oxidation level of aerosols increases.

3.1.3 Fluorescence characteristics of WSOC

The fluorescence spectroscopy analysis shows that urban sites (except NJ) have higher humidification index (HIX) values compared to regional sites (see Table 1 and Figure S5), suggesting that the fluorescence components in WSOC at urban sites have higher aromaticity than those at regional sites (Deng et al., 2022). The HIX values at urban sites are comparable to those of ambient aerosols and fresh biogenic SOA as well as aged SOA generated from the Maillard reaction reported in previous studies. However, the HIX values measured at the ten sites are overall much lower compared to those of aged biogenic SOA (Lee et al., 2013). This suggests that the contribution of aged biogenic SOA to fluorescence components is relatively small at each site during the wintertime. Moreover, the urban sites in Northern China (such as TJ, QD, XA, HD) exhibit higher biological index (BIX) and fluorescence index (FI) values compared to the urban sites in Southern China (such as CD, CQ, NJ) and regional sites (TS and HS). This suggests that primary combustion emissions such as biomass burning and coal combustion have higher influences on the fluorescent components in Northern China compared to Southern China and regional sites (Tang et al., 2021). It agrees well with different heating modes in north and south China in winter, and is also consistent

https://doi.org/10.5194/egusphere-2024-2416
Preprint. Discussion started: 20 August 2024

with the pollution sources at the regional sites.

The fluorophores in WSOC are further identified with the PARAFAC method. Five fluorophores (C1-C5) are resolved in TJ, four fluorophores (C1-C4) are resolved in QD, SH and HS, and three fluorophores (C1-C3) are resolved at other sites, respectively (see Figure S6). Therein, C1 at urban sites (TJ, HD, QD, NJ, SH, XA, CD, CQ) has a primary (secondary) Ex peak at around 250 nm (300 nm) with Em peak at around 395 nm, while Ex peak of C1 at regional sites (TS and HS) is at around 250 nm and 300 nm or 315 nm with Em peak at around 413 nm. Such fluorophores can be classified as less-oxygenated species (LO-HULIS) (Chen et al., 2016b). Moreover, the C4 resolved in TJ, QD, SH and HS are also considered as LO-HULIS for its main peak is distributed in the LO-HULIS region (Chen et al., 2020). Previous studies have reported that LO-HULIS is abundant in biomass burning aerosols, especially in winter (Jiang et al., 2022a). Additionally, industrial sources and other combustion related sources also make important contributions to LO-HULIS (Chen et al., 2020). C2 and C5 (only found in TJ) are with longer emission wavelengths (Em > 420 nm) and contain multiple Ex peaks (e.g., 250, 295, 305, 340, 345, 350, 355, 360, 370, 375 nm), and these fluorophores are regarded as highly-oxygenated species (HO-HULIS) (Chen et al., 2020). The multiple Ex peaks and longer Em peaks of HO-HULIS may be associated with aromatic conjugated structures and may contain heteroatoms (Chen et al., 2016a). HO-HULIS generally has a strong correlation with anthropogenic secondary formation and combustion emission (e.g., biomass burning and coal combustion) aerosols (Jiang et al., 2022b; Jiang et al., 2022a; Li et al., 2023b). Differently, C3 is mainly distributed in areas with lower Ex (260-275 nm) and Em (285-336 nm) wavelengths. Recent studies have shown that these fluorophores are compatible with the fluorescent peaks of amino acids (e.g., tyrosine, tryptophan) and non-N aromatic species (e.g., aromatic acids, phenolic compounds and their derivatives) (Chen et al., 2020; Cao et al., 2023). As concentrations of atmospheric amino acids are usually negligible, and the corresponding contribution to fluorophores is insignificant when compared to non-N aromatic species (Chen et al., 2020; Cao et al., 2023). Therefore, C3 is defined as non-N aromatic species (non-Nas) in this study, which is more likely derived from fossil fuel combustion (Tang et al., 2020; Li et al., 2023b).

Figure 3 illustrates the average fluorescence volume (FV) and relative contributions of the fluorophores at different sites. Generally, HULIS (LO-HULIS and HO-HULIS) components have the highest FV values and account for the highest proportion at most sites. Among them, LO-HULIS has the highest proportion (except for TS), followed by non-Nas, and HO-HULIS has the lowest proportion at most sites (except for TJ and TS). Notably, HO-HULIS is not resolved in TS, which corresponds to its low HIX. The FV of LO-HULIS and non-Nas in northern cities (LO-HULIS: 8436.99 ± 5680.49 RU-nm^2, non-Nas: 4410.09 ± 3165.82 RU-nm^2) are significantly higher ($p < 0.01$) than those in southern cities (LO-HULIS: 1841.11 ± 1452.71 RU-nm^2, non-Nas: 1860.12 ± 1103.52 RU-nm^2) and regional sites (LO-HULIS: 1091.96 ± 1703.56 RU-nm^2, non-Nas: 1797.01 ± 863.51 RU-nm^2), which can be attributed to the significant increase in combustion related anthropogenic emissions such as residential biomass burning during winter heating period in Northern China.

3.1.4 Functional group structural characteristics of WSOC

The structure of WSOC is further investigated by FTIR spectroscopy. The spectra of WSOC are generally similar at different

https://doi.org/10.5194/egusphere-2024-2416
Preprint. Discussion started: 20 August 2024

sites (see Figure 4). The FTIR spectra at each site mainly include six or seven absorption bands at 2635-3600 cm^{-1}, 1540-1820 cm^{-1}, 1220-1510 cm^{-1}, 977-1220 cm^{-1}, 860-960 cm^{-1}, 806-844 cm^{-1} and 590-727 cm^{-1}. The peak in the widest band at 2635-3600 cm^{-1} can be attributable to the intramolecular and intermolecular O-H stretching vibrations of alcohols, phenols and carboxylic acid (Wang et al., 2021; Fan et al., 2023; Huang et al., 2022). The peak in the band of 1540-1820 cm^{-1} is recognized as C=O stretching vibrations of carboxylic acids, ketones, aldehydes and esters (Wang et al., 2021; Fan et al., 2023; Yang et al., 2024). The sharp peak in the range of 1220-1510 cm^{-1} is attributed to C=C stretching vibrations of aromatic rings (Wang et al., 2021). The strongest peak occurs in the band of 977-1220 cm^{-1} can be assigned to C-O stretching vibrations of phenols, esters and ethers (Wang et al., 2021; Fan et al., 2023). The peak in the range of 860-960 cm^{-1} is only observed at some sites (i.e., TJ, HD, QD, CD and TS), which can be ascribed to C=C-H in alkenes (Yu et al., 2018). And the sharpest peak in the band of 806-844 cm^{-1} corresponds to R-ONO_2 stretching of organic nitrate (Huang et al., 2022), and multiple small peaks in the band at 590-727 cm^{-1} represent C-H bending vibrations of aromatic rings (Wang et al., 2021; Fan et al., 2023).

Quantitative analysis of functional groups is conducted by integrating peak area and the proportion of different functional groups at each site is presented in ring charts in Figure 4. Totally, O-H is the most abundant at all sites (39.2%-48.5%, the relative proportion), followed by C=C (16.6%-30.9%) and C-O (14.0%-27.8%). The proportion of C=C is generally higher at sites in Southern China than in Northern China, while C-O is the opposite. O-H and C=C are negatively correlated with E_2/E_3 (the ratio of the light absorption of WSOC at 250 nm and 365 nm, see Figure S7a and b). This indicates that these two functional groups may originate from aromatic compounds with higher molecular weight and higher degree of aromaticity, as lower E_2/E_3 values are related to higher aromaticity and molecular weight (Peuravuori and Pihlaja, 1997). To a certain extent, this can explain the strong light absorption capacity of WS-BrC in Northern China in winter. In contrast, the proportion of C-O and C=C-H (only detected at some sites) is positively correlated with E_2/E_3 (see Figure S7c and d), indicating that these two functional groups are mainly related to ester or ether and aliphatic hydrocarbon compounds with smaller molecular weights. The proportion of these two functional groups is significantly higher at the regional site in Northern China than at other sites. In contrast, C=O makes a greater contribution at the regional site in Southern China.

3.2 Identification of light-absorbing substances based on light absorption spectra

In order to further explore the light absorption characteristics of WSOC and their diversity at different sites, the absorption spectra (250-700 nm) of WSOC are analyzed and classified (see Figure 5). Clearly, there are significant differences in the absorption spectra at different sites. The light absorption coefficients (Abs_λ) of WSOC at each site exhibits strong wavelength dependence, especially over the UV-visible range (250-400 nm), which corresponds to the higher $AAE_{330\text{-}400}$ (4.07-9.17 on average). WSOC absorption spectra exhibit significant bimodal structures at 265 and 300 nm at sites in outside east China (e.g., TJ, HD, XA, CD, CQ, HS), which is different from the east China sites (e.g., QD, NJ, SH, TS), where absorption spectra decreased monotonically with the increase of wavelength. This indicates that there are significant differences in light-absorbing substances in WSOC in different regions. Therefore, the PMF-LAS method is used to analyze the potential categories of light absorbing substances. Based on this, the spectra measured in east China sites and outside east China sites are resolved into

https://doi.org/10.5194/egusphere-2024-2416
Preprint. Discussion started: 20 August 2024

four (eFac1, eFac2, eFac3, eFac4) and three (nFac1, nFac2, nFac3) light absorber factors, respectively (see Figure 6 and Figure S8).

By comparing with the light absorption spectra of BrC species in previous studies, the spectra resolved in this study are found to be similar to those of most aromatic or nitrogen-containing heterocyclic compounds. For example, eFac1 and nFac3 exhibit similar spectra, with clear absorption peaks at 320 nm or 350 nm and possibly stronger absorption peaks below 250 nm, which is consistent with the spectra of nitro-aromatic compounds such as 4-nitrocatechol (Lin et al., 2018; Huang et al., 2021; Yang et al., 2023). The absorbance of eFac2, eFac3 and nFac2 decreases sharply with increasing wavelength. eFac2 and nFac2 exhibit an absorption peak at 260 nm, while eFac3 shows no distinct peak. These factors are similar to the absorption spectra of nitro-aromatic compounds and nitrogen-free aromatic compounds, respectively (Jiang et al., 2022a; Cao et al., 2023). Additionally, eFac4 and nFac1 have a main absorption peak at around 290 nm and 300 nm, which match the absorption peak of most nitrogen-free aromatic compounds such as vanillin and a few nitro-aromatic compounds or nitrogen-containing heterocyclic compounds (Lin et al., 2018; Li et al., 2020; Huang et al., 2021; Yang et al., 2023). Taken together, the above spectral analysis suggests that the important light-absorbing components in WSOC may be mainly aromatic compounds. However, it is worth noting that this judgment is based on substances with known absorption spectra, and further studies on more kinds of absorption spectra are needed in the future.

The contributions of different light absorption factors and the leading contribution factors vary significantly at different wavelengths (see Figure S9). In east China, the absorption contribution of eFac1 from 250 to 400 nm decreases first and then increases, with the minimum contribution appearing around 290 nm, while the contribution trend of eFac4 is the opposite, with its maximum light absorption contribution occurring at 290 nm. The light absorption contribution of eFac2 is mainly concentrated within 340 nm and gradually decreases with the increase of wavelength. The eFac3 has a higher proportion of contribution at each wavelength and a smaller variation throughout the entire spectral range (250-400 nm), acting as the leading light absorption factor in the wavelength range below 350 nm. At outside east China sites, the maximum contribution of nFac1 to light absorption occurs at around 300 nm and gradually decreases thereafter, while the contribution of nFac3 is the opposite and increases after 300 nm. The contribution of nFac2 gradually decreases throughout the entire spectral range (250-400 nm), with overwhelming contribution below 350 nm especially at TJ, HD, CD, HS and CQ sites. The average contribution of each absorption factor to light absorption of WSOC over 250-400 nm wavelength at each site is shown in Figure 6. In general, the main absorption factor at east China sites is eFac3, and the major absorption factor is nFac2 at outside east China sites. eFac2, eFac3 and nFac2 (nitro-aromatic and nitrogen-free aromatic compounds) account for more than half (59.3%-80.0% and 17.9%-55.1%) of the light absorption. This suggests that nitro-aromatic or nitrogen-free aromatic compounds with strong wavelength dependence (e.g., 2-nitrobenzaldehyde) are the main light-absorbing species in the UV range in China, highlighting the importance of aromatic structure to WSOC light absorption.

The E_2/E_3 ratio calculated based on the light absorption spectra also shows that aromatic compounds are important light absorbers. As shown in Figure 7, E_2/E_3 values in north China, northwest China, and southwest China are relatively low, especially in XA, while the E_2/E_3 value at TS site is the highest. A very strong negative correlation between the Abs_{365} (r range:

https://doi.org/10.5194/egusphere-2024-2416
Preprint. Discussion started: 20 August 2024

-0.96 to -0.32, $p < 0.05$), MAE_{365} (r range: -0.83 to -0.32, $p < 0.05$) and E_2/E_3 values are observed. This further suggests that the strong light-absorbing ability of WSOC may be associated with more aromatic structures. A strong negative correlation ($p < 0.05$) is also found between E_2/E_3 and fluorophores, especially HULIS chromophores (see Figure S10), suggesting that the fluorophores also contain aromatic structures, and there may be a certain correlation between fluorophores and light-absorbing components, which will be discussed in the subsequent section.

3.3 Influencing factors of optical properties of WSOC

3.3.1 Variations of optical properties of WSOC with concentrations of $PM_{2.5}$ and gaseous pollutants

To investigate the influence by air quality levels on the light absorption properties of WSOC, the sampling days are classified into five pollution levels including clean (0-35 $\mu g \cdot m^{-3}$), relatively clean (35-75 $\mu g \cdot m^{-3}$), slightly polluted (75-115 $\mu g \cdot m^{-3}$), moderately polluted (115-150 $\mu g \cdot m^{-3}$), and heavily polluted (> 150 $\mu g \cdot m^{-3}$) according to the national ambient air quality daily Grade-II standard threshold values and ambient air quality indexes. As shown in Figure 8a, Abs_{365} of WSOC increased significantly with pollution levels, suggesting that the higher the degree of pollution, the higher the abundance of water-soluble BrC. The MAE_{365} values generally increase as the pollution level increases, especially under slightly pollution levels ($PM_{2.5} \leq$ 115 $\mu g \cdot m^{-3}$), and remain relatively stable under moderately and heavily polluted levels ($PM_{2.5}$ > 115 $\mu g \cdot m^{-3}$) (see Figure 8b). This may be due to the great changes in the composition and source of organic matter with the increase of pollution degrees from clean to low pollution (Li et al., 2019b), which tends to produce water-soluble organic matter with strong light absorption ability. In contrast, the increase of $PM_{2.5}$ concentration in highly polluted conditions is mainly due to the contribution of secondary inorganic components, while the chemical composition and sources of organic matter may remain relatively stable in the case of severe pollution and the processes of secondary formation and aging may lead to photobleaching or light enhancement, so that the light absorption capacity of WS-BrC may remain relatively stable (You et al., 2024).

The fluorescence volumes normalized by WSOC concentration (NFV) of different fluorophores exhibit different variation trend with $PM_{2.5}$ mass concentrations (see Figure 8c-e). The NFV of HO-HULIS fluorophore increases with $PM_{2.5}$ concentration, suggesting the increase of anthropogenic secondary formation and combustion emission (e.g., biomass burning and coal combustion) contributions with $PM_{2.5}$ pollution levels. By contrast, the NFV of non-Nas fluorophore decreases with $PM_{2.5}$ pollution levels, implying that the contributions of fossil fuel combustion may decrease under highly polluted conditions. As for LO-HULIS fluorophore, its NFV value is the highest during the clean days, with relatively lower values under polluted conditions but increasing trend with the pollution levels. The increase of NFV values of LO-HULIS further suggests that contributions from biomass burning increase under highly polluted conditions.

The relationships between conventional air pollutants (CO, NO_2, SO_2, O_3) and Abs_{365} are also analyzed. As shown in Figure S11, a strong positive correlation (r range: 0.40-0.93, $p < 0.05$) between Abs_{365} and CO, NO_2, SO_2 is observed in TJ, QD, SH, XA, CD, CQ and TS. As such air pollutants usually originate from fossil fuel combustion (e.g., coal combustion and vehicle emissions) or biomass burning (Adam et al., 2021), which suggests that the light absorption of WSOC in these regions could

https://doi.org/10.5194/egusphere-2024-2416
Preprint. Discussion started: 20 August 2024

be influenced by primary combustion. Among these air pollutants, CO and SO_2 have the greatest impact on Abs_{365} of WSOC (Figure S11c). A good negative correlation (*r* range: -0.66 to -0.40, $p < 0.05$) between Abs_{365} and O_3 is observed at TJ, QD, SH and XA. O_3 is typically considered a type of secondary air pollutant that can be generated through various pathways such as photochemical reactions (Adam et al., 2021). That means, the light absorption of WSOC at these sites may be also affected by atmospheric chemical processes (e.g., photo-bleaching) in addition to the primary combustion.

3.3.2 Variations of light absorption properties of WSOC with relative humidity (RH)

Figure 8f shows that MAE_{365} significantly decreases with increase of RH when RH is lower than 60%, while it exhibits no significant changes when RH > 60%. Previous studies have indicated that the mixed particles containing 4-nitrophenol and ammonium sulfate will undergo phase separation, and the separated core-shell particles may enhance light absorption through the lensing effect at low RH (Price et al., 2022; Liu et al., 2023). Moreover, compared to dry conditions, the loss of BrC light absorption is faster at high RH. It has been reported that non-phenolic aromatic carbonyls may undergo aqueous-phase photo-oxidation to produce H_2O_2, which can be further decomposed to produce OH radicals at high RH, and OH radicals will bleach the BrC chromophore (Zhong and Jang, 2014; Anastasio et al., 1997; Faust, 1994; Zellner et al., 1990). Therefore, the decreasing MAE_{365} with increased RH may be related to phase changes, photo-bleaching processes as well as the changes in BrC chromophores.

3.4 Relationships among fluorescent chromophore, functional groups and light absorption of WSOC

To better understand the relationships among light absorption, fluorescence and functional group structure of WS-BrC, several correlation analysis methods are used. Figure S10 shows that Abs_{365} strongly correlated with the TFV of fluorophores at all sites ($p < 0.01$), indicating that the fluorescent components may contribute to WOSC light absorption to some extent. Then, MLR model is applied to evaluate the relationship between the maximum fluorescence intensity (F_{max}) of various fluorescent components and Abs_{365}, and a good linear fitting relationship is found between measured Abs_{365} and modeled Abs_{365} (see Figure 9). The adjusted R^2 values of the MLR model range from 0.62 to 0.93, implying that the fluorophores measured can explain 61.8%-93.0% of the measured WSOC light absorption. Furthermore, the contribution of various fluorophores to Abs_{365} is quantified by calculating the standardized regression coefficients (*Beta*) in the MLR model (see the circular graph in Figure 9). The results show that HULIS fluorophores have the greatest contribution to Abs_{365}, with higher contributions by HO-HULIS (28.5%-49.7%) than LO-HULIS (15.2%-59.6%) and followed by non-Nas (0.3%-25.8%), although HO-HULIS has accounts for the lowest proportion of the total fluorophores. The high contribution of HO-HULIS to Abs_{365} may be related to its complex source and composition, such as the presence of unsaturated and high molecular weight aromatic structures in HO-HULIS. Previous studies have shown that the light-absorbing ability of BrC is positively correlated with the unsaturation and molecular weight of chromophores (Tang et al., 2020; Chen and Bond, 2010). It should be noted that the situation is different at TS site, where HO-HULIS is not resolved, and the contribution of LO-HULIS to Abs_{365} at TS site is much higher than that of non-Nas (59.6% > 2.2%). To better understand the importance of fluorophores to WSOC light absorption, the fluorescence intensity of

https://doi.org/10.5194/egusphere-2024-2416
Preprint. Discussion started: 20 August 2024

each fluorophore at all sites is summarized and input into the XGBoost-SHAP model. The absolute value of the average SHAP score is used to evaluate the importance of different fluorophores on Abs_{365}, with the larger the value, the greater its importance. As shown in Figure S12, HO-HULIS is of the highest importance, much higher than non-Nas and LO-HULIS. This further demonstrates the important contribution of fluorescent components to light absorption of WSOC, especially HO-HULIS.

Figure 10 illustrates the relationships of light absorption parameters and fluorescence chromophores with functional groups. In general, fluorescence chromophores (especially the HULIS classes) and the Abs_{365} exhibit similar correlations with functional groups at all sites, which agrees well with the important contribution of fluorescence chromophores to the light absorption of WSOC as aforementioned. At most sites (except XA and CQ), O-H, C=C and R-ONO_2 functional groups show the strongest positive correlations with Abs_{365} and fluorescent chromophores, implying that aromatic compounds (especially at polluted sites such as HD, NJ, QD, and CD) and organic nitrates (especially at less polluted sites such as SH, TS and HS) have important impacts on the optical properties of WSOC. However, ester or ether and aliphatic hydrocarbon functional groups (e.g., C-O and C=C-H) have relatively smaller positive impacts on the optical properties of WSOC, even exhibiting negative correlations with light absorption parameters and fluorescence chromophores at some sites. In contrast, the relationships between MAE_{365} values and functional groups may differ from Abs_{365}. Similarly, C=C, O-H and R-ONO_2 exhibit the strongest correlations with MAE_{365} at most sites (e.g., TJ, QD, SH, TS, and HS). However, C=O and C-O, which might be related to carboxylic acids, phenols and esters, may also have a positive correlation with MAE_{365} at other sites (e.g., HD, NJ, XA, CQ). The positive correlation of C=O and C-H functional groups with both Abs_{365} and MAE_{365} and the strong positive correlation of C-O group with MAE_{365} in XA could explain the particularity of light absorption characteristics and the ability of WS-BrC in XA to a certain extent.

4 Conclusions

Based on the same measurement methods and data processing processes, light absorption, fluorescence and FTIR spectra analysis are combined to investigate the optical properties and functional group characteristics of WSOC at ten sites in different regions of China, and the discrepancies at various sites and the relationships between absorbance, fluorescence, and functional groups of WSOC are revealed. Mass concentrations of carbonaceous components (OC, EC and WSOC) and light absorption of WSOC exhibit a significant spatial variation at the ten sites, which generally manifested as northwest China > southwest China > north China > east China > regional site, with higher values in Northern China than Southern China and regional sites, and higher in inland areas than coastal areas.

The aromatic and large molecular weight structure has a significant impact on the light-absorbing ability of WSOC according to the E_2/E_3 ratio, PMF-LAS resolved light absorption factors and functional groups. PMF-LAS method determines four (eFac1-eFac4) and three (nFac1-nFac3) light absorption factors in east and outside east China, respectively, which are mainly aromatic compounds by comparing the spectra with existing BrC species. Furthermore, FTIR based function groups show that aromatic O-H (39.2%-48.5%) and C=C (16.6%-30.9%), as well as aliphatic C-O (14.0%-27.8%) are three most abundant

https://doi.org/10.5194/egusphere-2024-2416
Preprint. Discussion started: 20 August 2024

functional groups in WSOC. The strong positive correlation between aromatic O-H and C=C with Abs_{365} and MAE_{365} suggests that aromatic components (especially phenolic compounds) play an important role in the light absorption of WSOC. Three types of fluorophores in WSOC are resolved by PARAFAC analysis, with LO-HULIS as the most abundant fluorophore, followed by non-Nas and HO-HULIS. The positive correlation between E_2/E_3 and aromatic functional groups (O-H and C=C) with these fluorescent chromophores indicates that aromatic structures also have an important impact on the fluorescent components. This also indicates that there is an undeniable connection between the light absorption and fluorescence of WSOC. Quantitatively, MLR results show that the identified fluorophores contribute significantly (61.8%-93.0%) to the Abs_{365} of WSOC, especially HULIS (LO-HULIS and HO-HULIS), with the largest contribution by HO-HULIS (28.5%-49.7%). Analysis of the relationships between WSOC light absorption and gaseous precursors and meteorological conditions show that primary combustion sources have significant impacts on WSOC light absorption at most sites (such as TJ, QD, SH, XA, CD, CQ and TS), and atmospheric chemical process (such as photobleaching) exhibit more effects on WSOC light absorption at TJ, QD, SH and XA sites. Moreover, the multi-site observation dataset shows that MAE_{365} of WSOC generally increases with pollution levels and decreases with increasing RH within the range of 20%-60% and keeps stable when RH > 60%. Taken together, this study promotes our knowledge of optical properties and structural characteristics of WSOC in different regions of China and deepened the understanding of the contribution of WSOC fluorescence to its light absorption. In the future, it is necessary to build a quantitative parametric relationship between light absorption, composition and structure of WSOC, especially with the evolution of atmospheric processes.

Data availability. Data presented and used throughout this study can be accessed from the following data repository: https://doi.org/10.5281/zenodo.13144297 (Chen, 2024).

Supplement. The supplement includes six texts (Texts S1-S6), two tables (Tables S1-S2) and twelve figures (Figure S1-S12) related to the paper.

Author contributions. CY designed the research and supported funding the observation. XW, QC, MX, JL, FW, SF, QY, HN, MZ, YW and LX had an active role in supporting the sampling work. HC carried out the sample pretreatment and instrumental analysis under the guidance of CY, LH and LD. HC processed data, plotted the figures, and wrote the manuscript. YY provided assistance in data processing. CY edited the manuscript. All authors contributed to the discussions of the results and the refinement of the manuscript.

Competing interests. The authors declare no conflicts of interest.

https://doi.org/10.5194/egusphere-2024-2416
Preprint. Discussion started: 20 August 2024

Financial support. This work was supported by the Natural Science Foundation of China (NO. 4225110), Natural Science Foundation of Shandong Province (ZR2021MD033), Natural Science Foundation of Jiangsu Province (BK20220275), the Excellent Young Scholar (Overseas) project of Shandong Province (2022HWYQ-049), Open fund by Jiangsu Key Laboratory of Atmospheric Environment Monitoring and Pollution Control (KHK2106), and Taishan Scholars Program of Shandong Province (NO. tsqn201909018) and Qilu Youth Talent of Shandong University.

References

Adam, M. G., Tran, P. T. M., and Balasubramanian, R.: Air quality changes in cities during the COVID-19 lockdown: A critical review, Atmospheric Research, 264, 105823, https://doi.org/10.1016/j.atmosres.2021.105823, 2021.

Anastasio, C., Faust, B. C., and Rao, C. J.: Aromatic carbonyl compounds as aqueous-phase photochemical sources of hydrogen peroxide in acidic sulfate aerosols, fogs, and clouds. 1. Non-phenolic methoxybenzaldehydes and methoxyacetophenones with reductants (phenols), Environmental Science & Technology, 31, 218-232, https://doi.org/10.1021/es960359g, 1997.

Andreae, M. O. and Gelencsér, A.: Black carbon or brown carbon? The nature of light-absorbing carbonaceous aerosols, Atmospheric Chemistry and Physics, 6, 3131-3148, https://doi.org/10.5194/acp-6-3131-2006, 2006.

Bosch, C., Andersson, A., Kirillova, E. N., Budhavant, K., Tiwari, S., Praveen, P. S., Russell, L. M., Beres, N. D., Ramanathan, V., and Gustafsson, O.: Source-diagnostic dual-isotope composition and optical properties of water-soluble organic carbon and elemental carbon in the South Asian outflow intercepted over the Indian Ocean, Journal of Geophysical Research: Atmospheres, 119, 11743-11759, https://doi.org/10.1002/2014jd022127, 2014.

Cao, T., Li, M., Xu, C., Song, J., Fan, X., Li, J., Jia, W., and Peng, P. a.: Technical note: Chemical composition and source identification of fluorescent components in atmospheric water-soluble brown carbon by excitation-emission matrix spectroscopy with parallel factor analysis-potential limitations and applications, Atmospheric Chemistry and Physics, 23, 2613-2625, https://doi.org/10.5194/acp-23-2613-2023, 2023.

Cao, X., Liu, J., Wu, Y., Cheng, Y., Zheng, M., and He, K.: A review on brown carbon aerosol in China: From molecular composition to climate impact, Current Pollution Reports, 10, 326-343, https://doi.org/10.1007/s40726-024-00293-y, 2024.

Chen, H., Zhou, R., Fang, L., Sun, H., Yang, Q., Niu, H., Liu, J., Tian, Y., Cui, M., and Yan, C.: Variations in optical properties of water- and methanol-soluble organic carbon in $PM_{2.5}$ in Tianjin and Handan over the wintertime of 2018-2020, Atmospheric Research, 303, 107332, https://doi.org/10.1016/j.atmosres.2024.107332, 2024.

Chen, H., Yan, C., Fu, Q., Wang, X., Tang, J., Jiang, B., Sun, H., Luan, T., Yang, Q., Zhao, Q., Li, J., Zhang, G., Zheng, M., Zhou, X., Chen, B., Du, L., Zhou, R., Zhou, T., and Xue, L.: Optical properties and molecular composition of wintertime atmospheric water-soluble organic carbon in different coastal cities of eastern China, Science of the Total Environment, 892, 164702, https://doi.org/10.1016/j.scitotenv.2023.164702, 2023.

Chen, Q., Ikemori, F., and Mochida, M.: Light absorption and excitation-emission fluorescence of urban organic aerosol

https://doi.org/10.5194/egusphere-2024-2416
Preprint. Discussion started: 20 August 2024

components and their relationship to chemical structure, Environmental Science & Technology, 50, 10859-10868, https://doi.org/10.1021/acs.est.6b02541, 2016a.

Chen, Q., Wang, M., Wang, Y., Zhang, L., Li, Y., and Han, Y.: Oxidative potential of water-soluble matter associated with chromophoric substances in $PM_{2.5}$ over Xi'an, China, Environmental Science & Technology, 53, 8574-8584, https://doi.org/10.1021/acs.est.9b01976, 2019.

Chen, Q., Li, J., Hua, X., Jiang, X., Mu, Z., Wang, M., Wang, J., Shan, M., Yang, X., Fan, X., Song, J., Wang, Y., Guan, D., and Du, L.: Identification of species and sources of atmospheric chromophores by fluorescence excitation-emission matrix with parallel factor analysis, Science of the Total Environment, 718, 137322, https://doi.org/10.1016/j.scitotenv.2020.137322, 2020.

Chen, Q., Miyazaki, Y., Kawamura, K., Matsumoto, K., Coburn, S., Volkamer, R., Iwamoto, Y., Kagami, S., Deng, Y., Ogawa, S., Ramasamy, S., Kato, S., Ida, A., Kajii, Y., and Mochida, M.: Characterization of chromophoric water-soluble organic matter in urban, forest, and marine aerosols by HR-ToF-AMS analysis and excitation-emission matrix spectroscopy, Environmental Science & Technology, 50, 10351-10360, https://doi.org/10.1021/acs.est.6b01643, 2016b.

Chen, Y. and Bond, T. C.: Light absorption by organic carbon from wood combustion, Atmospheric Chemistry and Physics, 10, 1773-1787, https://doi.org/10.5194/acp-10-1773-2010, 2010.

Chen, Y. F., Ge, X. L., Chen, H., Xie, X. C., Chen, Y. T., Wang, J. F., Ye, Z. L., Bao, M. Y., Zhang, Y. L., and Chen, M. D.: Seasonal light absorption properties of water-soluble brown carbon in atmospheric fine particles in Nanjing, China, Atmospheric Environment, 187, 230-240, https://doi.org/10.1016/j.atmosenv.2018.06.002, 2018.

Cheng, Y., He, K. B., Du, Z. Y., Engling, G., Liu, J. M., Ma, Y. L., Zheng, M., and Weber, R. J.: The characteristics of brown carbon aerosol during winter in Beijing, Atmospheric Environment, 127, 355-364, https://doi.org/10.1016/j.atmosenv.2015.12.035, 2016.

Cheng, Y., He, K. B., Zheng, M., Duan, F., Du, Z. Y., Ma, Y. L., Tan, J. H., Yang, F. M., Liu, J. M., Zhang, X. L., Weber, R. J., Bergin, M. H., and Russell, A. G.: Mass absorption efficiency of elemental carbon and water-soluble organic carbon in Beijing, China, Atmospheric Chemistry and Physics, 11, 11497-11510, https://doi.org/10.5194/acp-11-11497-2011, 2011.

Choudhary, V., Rajput, P., and Gupta, T.: Absorption properties and forcing efficiency of light-absorbing water-soluble organic aerosols: Seasonal and spatial variability, Environmental Pollution, 272, 115932, https://doi.org/10.1016/j.envpol.2020.115932, 2021.

Deng, J., Ma, H., Wang, X., Zhong, S., Zhang, Z., Zhu, J., Fan, Y., Hu, W., Wu, L., Li, X., Ren, L., Pavuluri, C. M., Pan, X., Sun, Y., Wang, Z., Kawamura, K., and Fu, P.: Measurement report: Optical properties and sources of water-soluble brown carbon in Tianjin, North China-insights from organic molecular compositions, Atmospheric Chemistry and Physics, 22, 6449-6470, https://doi.org/10.5194/acp-22-6449-2022, 2022.

Dey, S. and Sarkar, S.: Compositional and optical characteristics of aqueous brown carbon and HULIS in the eastern Indo-Gangetic Plain using a coupled EEM PARAFAC, FT-IR and ^{1}H NMR approach, Science of The Total Environment, 921, 171084, https://doi.org/10.1016/j.scitotenv.2024.171084, 2024.

https://doi.org/10.5194/egusphere-2024-2416
Preprint. Discussion started: 20 August 2024

Dey, S., Mukherjee, A., Polana, A. J., Rana, A., Mao, J., Jia, S., Yadav, A. K., Khillare, P. S., and Sarkar, S.: Brown carbon aerosols in the Indo-Gangetic Plain outflow: Insights from excitation emission matrix (EEM) fluorescence spectroscopy, Environmental Science Processes & Impacts, 23, 745-755, https://doi.org/10.1039/d1em00050k, 2021.

Diesch, J. M., Drewnick, F., Zorn, S. R., von der Weiden-Reinmüller, S. L., Martinez, M., and Borrmann, S.: Variability of aerosol, gaseous pollutants and meteorological characteristics associated with changes in air mass origin at the SW Atlantic coast of Iberia, Atmospheric Chemistry and Physics, 12, 3761-3782, https://doi.org/10.5194/acp-12-3761-2012, 2012.

Fan, X., Cheng, A., Chen, D., Cao, T., Ji, W., Song, J., and Peng, P.: Investigating the molecular weight distribution of atmospheric water-soluble brown carbon using high-performance size exclusion chromatography coupled with diode array and fluorescence detectors, Chemosphere, 338, 139517, https://doi.org/10.1016/j.chemosphere.2023.139517, 2023.

Fan, X. J., Wei, S. Y., Zhu, M. B., Song, J. Z., and Peng, P. A.: Comprehensive characterization of humic-like substances in smoke $PM_{2.5}$ emitted from the combustion of biomass materials and fossil fuels, Atmospheric Chemistry and Physics, 16, 13321-13340, https://doi.org/10.5194/acp-16-13321-2016, 2016.

Fang, W., Andersson, A., Lee, M., Zheng, M., Du, K., Kim, S.-W., Holmstrand, H., and Gustafsson, Ö.: Combined influences of sources and atmospheric bleaching on light absorption of water-soluble brown carbon aerosols, npj Climate and Atmospheric Science, 6, 104, https://doi.org/10.1038/s41612-023-00438-8, 2023.

Faust, B. C.: Photochemistry of clouds, fogs, and aerosols, Environmental Science & Technology, 28, 217-222, https://doi.org/10.1021/es00054a001, 1994.

Hecobian, A., Zhang, X., Zheng, M., Frank, N., Edgerton, E. S., and Weber, R. J.: Water-soluble organic aerosol material and the light-absorption characteristics of aqueous extracts measured over the Southeastern United States, Atmospheric Chemistry and Physics, 10, 5965-5977, https://doi.org/10.5194/acp-10-5965-2010, 2010.

Huang, R.-J., Yang, L., Shen, J., Yuan, W., Gong, Y., Ni, H., Duan, J., Yan, J., Huang, H., You, Q., and Li, Y. J.: Chromophoric fingerprinting of brown carbon from residential biomass burning, Environmental Science & Technology Letters, 9, 102-111, https://doi.org/10.1021/acs.estlett.1c00837, 2021.

Huang, R. J., Yang, L., Cao, J., Chen, Y., Chen, Q., Li, Y., Duan, J., Zhu, C., Dai, W., Wang, K., Lin, C., Ni, H., Corbin, J. C., Wu, Y., Zhang, R., Tie, X., Hoffmann, T., O'Dowd, C., and Dusek, U.: Brown carbon aerosol in urban Xi'an, northwest China: The composition and light absorption properties, Environmental Science & Technology, 52, 6825-6833, https://doi.org/10.1021/acs.est.8b02386, 2018.

Huang, S., Luo, Y., Wang, X., Zhang, T., Lei, Y., Zeng, Y., Sun, J., Che, H., Xu, H., Cao, J., and Shen, Z.: Optical properties, chemical functional group, and oxidative activity of different polarity levels of water-soluble organic matter in $PM_{2.5}$ from biomass and coal combustion in rural areas in Northwest China, Atmospheric Environment, 283, 119179, https://doi.org/10.1016/j.atmosenv.2022.119179, 2022.

Jiang, F., Song, J., Bauer, J., Gao, L., Vallon, M., Gebhardt, R., Leisner, T., Norra, S., and Saathoff, H.: Chromophores and chemical composition of brown carbon characterized at an urban kerbside by excitation-emission spectroscopy and mass spectrometry, Atmospheric Chemistry and Physics, 22, 14971-14986, https://doi.org/10.5194/acp-22-14971-2022, 2022a.

https://doi.org/10.5194/egusphere-2024-2416
Preprint. Discussion started: 20 August 2024

Jiang, H. X., Tang, J., Li, J., Zhao, S. Z., Mo, Y. Z., Tian, C. G., Zhang, X. Y., Jiang, B., Liao, Y. H., Chen, Y. J., and Zhang, G.: Molecular signatures and sources of fluorescent components in atmospheric organic matter in south China, Environmental Science & Technology Letters, 9, 913-920, https://doi.org/10.1021/acs.estlett.2c00629, 2022b.

Jiang, Y., Xue, L., Gu, R., Jia, M., Zhang, Y., Wen, L., Zheng, P., Chen, T., Li, H., Shan, Y., Zhao, Y., Guo, Z., Bi, Y., Liu, H., Ding, A., Zhang, Q., and Wang, W.: Sources of nitrous acid (HONO) in the upper boundary layer and lower free troposphere of the North China Plain: Insights from the Mount Tai Observatory, Atmospheric Chemistry and Physics, 20, 12115-12131, https://doi.org/10.5194/acp-20-12115-2020, 2020.

Kirillova, E. N., Andersson, A., Tiwari, S., Srivastava, A. K., Bisht, D. S., and Gustafsson, O.: Water-soluble organic carbon aerosols during a full New Delhi winter: Isotope-based source apportionment and optical properties, Journal of Geophysical Research: Atmospheres, 119, 3476-3485, https://doi.org/10.1002/2013jd020041, 2014.

Kirillova, E. N., Marinoni, A., Bonasoni, P., Vuillermoz, E., Facchini, M. C., Fuzzi, S., and Decesari, S.: Light absorption properties of brown carbon in the high Himalayas, Journal of Geophysical Research: Atmospheres, 121, 9621-9639, https://doi.org/10.1002/2016jd025030, 2016.

Laskin, A., Laskin, J., and Nizkorodov, S. A.: Chemistry of atmospheric brown carbon, Chemical Reviews, 115, 4335-4382, https://doi.org/10.1021/cr5006167, 2015.

Lee, H. J., Laskin, A., Laskin, J., and Nizkorodov, S. A.: Excitation-emission spectra and fluorescence quantum yields for fresh and aged biogenic secondary organic aerosols, Environmental Science & Technology, 47, 5763-5770, https://doi.org/10.1021/es400644c, 2013.

Li, C., He, Q., Schade, J., Passig, J., Zimmermann, R., Meidan, D., Laskin, A., and Rudich, Y.: Dynamic changes in optical and chemical properties of tar ball aerosols by atmospheric photochemical aging, Atmospheric Chemistry and Physics, 19, 139-163, https://doi.org/10.5194/acp-19-139-2019, 2019a.

Li, D., Wu, C., Zhang, S., Lei, Y., Lv, S., Du, W., Liu, S., Zhang, F., Liu, X., Liu, L., Meng, J., Wang, Y., Gao, J., and Wang, G.: Significant coal combustion contribution to water-soluble brown carbon during winter in Xingtai, China: Optical properties and sources, Journal of Environmental Sciences, 124, 892-900, https://doi.org/10.1016/j.jes.2022.02.026, 2023a.

Li, H., Cheng, J., Zhang, Q., Zheng, B., Zhang, Y., Zheng, G., and He, K.: Rapid transition in winter aerosol composition in Beijing from 2014 to 2017: response to clean air actions, Atmospheric Chemistry and Physics, 19, 11485-11499, https://doi.org/10.5194/acp-19-11485-2019, 2019b.

Li, P., Yue, S., Yang, X., Liu, D., Zhang, Q., Hu, W., Hou, S., Zhao, W., Ren, H., Li, G., Gao, Y., Deng, J., Xie, Q., Sun, Y., Wang, Z., and Fu, P.: Fluorescence properties and chemical composition of fine particles in the background atmosphere of North China, Advances in Atmospheric Sciences, 40, 1159-1174, https://doi.org/10.1007/s00376-022-2208-x, 2023b.

Li, R., Yan, C., Meng, Q., Yue, Y., Jiang, W., Yang, L., Zhu, Y., Xue, L., Gao, S., Liu, W., Chen, T., and Meng, J.: Key toxic components and sources affecting oxidative potential of atmospheric particulate matter using interpretable machine learning: Insights from fog episodes, Journal of Hazardous Materials, 465, 133175, https://doi.org/10.1016/j.jhazmat.2023.133175, 2024.

Li, X., Wang, Y. J., Hu, M., Tan, T. Y., Li, M. R., Wu, Z. J., Chen, S. Y., and Tang, X. Y.: Characterizing chemical composition

https://doi.org/10.5194/egusphere-2024-2416
Preprint. Discussion started: 20 August 2024

and light absorption of nitroaromatic compounds in the winter of Beijing, Atmospheric Environment, 237, 117712, https://doi.org/10.1016/j.atmosenv.2020.117712, 2020.

Li, X., Yu, F., Song, Y., Zhang, C., Yan, F., Hu, Z., Lei, Y., Tripathee, L., Zhang, R., Guo, J., Wang, Y., Chen, Q., Liu, L., Cao, J., and Wang, Q.: Water-soluble brown carbon in $PM_{2.5}$ at two typical sites in Guanzhong Basin: Optical properties, sources, and implications, Atmospheric Research, 281, 106499, https://doi.org/10.1016/j.atmosres.2022.106499, 2023c.

Lin, P., Fleming, L. T., Nizkorodov, S. A., Laskin, J., and Laskin, A.: Comprehensive molecular characterization of atmospheric brown carbon by high resolution mass spectrometry with electrospray and atmospheric pressure photoionization, Analytical Chemistry, 90, 12493-12502, https://doi.org/10.1021/acs.analchem.8b02177, 2018.

Liu, J., Mo, Y., Ding, P., Li, J., Shen, C., and Zhang, G.: Dual carbon isotopes (^{14}C and ^{13}C) and optical properties of WSOC and HULIS-C during winter in Guangzhou, China, Science of the Total Environment, 633, 1571-1578, https://doi.org/10.1016/j.scitotenv.2018.03.293, 2018.

Liu, X., Wang, H., Wang, F., Lv, S., Wu, C., Zhao, Y., Zhang, S., Liu, S., Xu, X., Lei, Y., and Wang, G.: Secondary formation of atmospheric brown carbon in China haze: Implication for an enhancing role of ammonia, Environmental Science & Technology, 57, 11163-11172, https://doi.org/10.1021/acs.est.3c03948, 2023.

Liu, X. Y., Zhang, Y. L., Peng, Y. R., Xu, L. L., Zhu, C. M., Cao, F., Zhai, X. Y., Haque, M. M., Yang, C., Chang, Y. H., Huang, T., Xu, Z. F., Bao, M. Y., Zhang, W. Q., Fan, M. Y., and Lee, X. H.: Chemical and optical properties of carbonaceous aerosols in Nanjing, eastern China: Regionally transported biomass burning contribution, Atmospheric Chemistry and Physics, 19, 11213-11233, https://doi.org/10.5194/acp-19-11213-2019, 2019.

Niu, X., Pu, W., Fu, P., Chen, Y., Xing, Y., Wu, D., Chen, Z., Shi, T., Zhou, Y., Wen, H., and Wang, X.: Fluorescence characteristics, absorption properties, and radiative effects of water-soluble organic carbon in seasonal snow across northeastern China, Atmospheric Chemistry and Physics, 22, 14075-14094, https://doi.org/10.5194/acp-22-14075-2022, 2022.

Peuravuori, J. and Pihlaja, K.: Molecular size distribution and spectroscopic properties of aquatic humic substances, Analytica Chimica Acta, 337, 133-149, https://doi.org/10.1016/s0003-2670(96)00412-6, 1997.

Price, C. L., Preston, T. C., and Davies, J. F.: Hygroscopic growth, phase morphology, and optical properties of model aqueous brown carbon aerosol, Environmental Science & Technology, 56, 3941-3951, https://doi.org/10.1021/acs.est.1c07356, 2022.

Ram, K., Sarin, M. M., and Tripathi, S. N.: Temporal trends in atmospheric $PM_{2.5}$, PM_{10}, elemental carbon, organic carbon, water-soluble organic carbon, and optical properties: Impact of biomass burning emissions in the Indo-Gangetic Plain, Environmental Science & Technology, 46, 686-695, https://doi.org/10.1021/es202857w, 2012.

Soleimanian, E., Mousavi, A., Taghvaee, S., Shafer, M. M., and Sioutas, C.: Impact of secondary and primary particulate matter (PM) sources on the enhanced light absorption by brown carbon (BrC) particles in central Los Angeles, Science of the Total Environment, 705, 135902, https://doi.org/10.1016/j.scitotenv.2019.135902, 2020.

Srinivas, B. and Sarin, M. M.: Light absorbing organic aerosols (brown carbon) over the tropical Indian Ocean: impact of biomass burning emissions, Environmental Research Letters, 8, 044042, https://doi.org/10.1088/1748-9326/8/4/044042, 2013.

Srinivas, B. and Sarin, M. M.: Brown carbon in atmospheric outflow from the Indo-Gangetic Plain: Mass absorption efficiency

https://doi.org/10.5194/egusphere-2024-2416
Preprint. Discussion started: 20 August 2024

and temporal variability, Atmospheric Environment, 89, 835-843, https://doi.org/10.1016/j.atmosenv.2014.03.030, 2014.

Srinivas, B., Rastogi, N., Sarin, M. M., Singh, A., and Singh, D.: Mass absorption efficiency of light absorbing organic aerosols from source region of paddy-residue burning emissions in the Indo-Gangetic Plain, Atmospheric Environment, 125, 360-370, https://doi.org/10.1016/j.atmosenv.2015.07.017, 2016.

Tang, J., Li, J., Su, T., Han, Y., Mo, Y. Z., Jiang, H. X., Cui, M., Jiang, B., Chen, Y. J., Tang, J. H., Song, J. Z., Peng, P. A., and Zhang, G.: Molecular compositions and optical properties of dissolved brown carbon in biomass burning, coal combustion, and vehicle emission aerosols illuminated by excitation-emission matrix spectroscopy and Fourier transform ion cyclotron resonance mass spectrometry analysis, Atmospheric Chemistry and Physics, 20, 2513-2532, https://doi.org/10.5194/acp-20-2513-2020, 2020.

Tang, J., Wang, J. Q., Zhong, G. C., Jiang, H. X., Mo, Y. Z., Zhang, B. L., Geng, X. F., Chen, Y. J., Tang, J. H., Tian, C. G., Bualert, S., Li, J., and Zhang, G.: Measurement report: Long-emission-wavelength chromophores dominate the light absorption of brown carbon in aerosols over Bangkok: Impact from biomass burning, Atmospheric Chemistry and Physics, 21, 11337-11352, https://doi.org/10.5194/acp-21-11337-2021, 2021.

Teich, M., van Pinxteren, D., Wang, M., Kecorius, S., Wang, Z. B., Muller, T., Mocnik, G., and Herrmann, H.: Contributions of nitrated aromatic compounds to the light absorption of water-soluble and particulate brown carbon in different atmospheric environments in Germany and China, Atmospheric Chemistry and Physics, 17, 1653-1672, https://doi.org/10.5194/acp-17-1653-2017, 2017.

Ting, Y.-C., Ko, Y.-R., Huang, C.-H., Cheng, Y.-H., and Huang, C.-H.: Optical properties and potential sources of water-soluble and methanol-soluble organic aerosols in Taipei, Taiwan, Atmospheric Environment, 290, 119364, https://doi.org/10.1016/j.atmosenv.2022.119364, 2022.

Wang, D., Shen, Z., Zhang, Q., Lei, Y., Zhang, T., Huang, S., Sun, J., Xu, H., and Cao, J.: Winter brown carbon over six of China's megacities: Light absorption, molecular characterization, and improved source apportionment revealed by multilayer perceptron neural network, Atmospheric Chemistry and Physics, 22, 14893-14904, https://doi.org/10.5194/acp-22-14893-2022, 2022a.

Wang, L., Zhou, X., Ma, Y., Cao, Z., Wu, R., and Wang, W.: Carbonaceous aerosols over China-review of observations, emissions, and climate forcing, Environmental Science and Pollution Research, 23, 1671-1680, https://doi.org/10.1007/s11356-015-5398-2, 2016.

Wang, Q., Zhou, Y., Ma, N., Zhu, Y., Zhao, X., Zhu, S., Tao, J., Hong, J., Wu, W., Cheng, Y., and Su, H.: Review of brown carbon aerosols in China: Pollution level, optical properties, and emissions, Journal of Geophysical Research: Atmospheres, 127, e2021JD035473, https://doi.org/10.1029/2021jd035473, 2022b.

Wang, X., Heald, C. L., Liu, J., Weber, R. J., Campuzano-Jost, P., Jimenez, J. L., Schwarz, J. P., and Perring, A. E.: Exploring the observational constraints on the simulation of brown carbon, Atmospheric Chemistry and Physics, 18, 635-653, https://doi.org/10.5194/acp-18-635-2018, 2018.

Wang, X., Qin, Y., Qin, J., Long, X., Qi, T., Chen, R., Xiao, K., and Tan, J.: Spectroscopic insight into the pH-dependent

https://doi.org/10.5194/egusphere-2024-2416
Preprint. Discussion started: 20 August 2024

interactions between atmospheric heavy metals (Cu and Zn) and water-soluble organic compounds in $PM_{2.5}$, Science of the Total Environment, 767, 145261, https://doi.org/10.1016/j.scitotenv.2021.145261, 2021.

Wu, G., Fu, P., Ram, K., Song, J., Chen, Q., Kawamura, K., Wan, X., Kang, S., Wang, X., Laskin, A., and Cong, Z.: Fluorescence characteristics of water-soluble organic carbon in atmospheric aerosol, Environmental Pollution, 268, 115906, https://doi.org/10.1016/j.envpol.2020.115906, 2021.

Wu, G., Wan, X., Ram, K., Li, P., Liu, B., Yin, Y., Fu, P., Loewen, M., Gao, S., Kang, S., Kawamura, K., Wang, Y., and Cong, Z.: Light absorption, fluorescence properties and sources of brown carbon aerosols in the Southeast Tibetan Plateau, Environmental Pollution, 257, 113616, https://doi.org/10.1016/j.envpol.2019.113616, 2020.

Xie, X., Chen, Y., Nie, D., Liu, Y., Liu, Y., Lei, R., Zhao, X., Li, H., and Ge, X.: Light-absorbing and fluorescent properties of atmospheric brown carbon: A case study in Nanjing, China, Chemosphere, 251, 126350, https://doi.org/10.1016/j.chemosphere.2020.126350, 2020.

Xu, J., Hettiyadura, A. P. S., Liu, Y., Zhang, X., Kang, S., and Laskin, A.: Regional differences of chemical composition and optical properties of aerosols in the Tibetan Plateau, Journal of Geophysical Research: Atmospheres, 125, e2019JD031226, https://doi.org/10.1029/2019jd031226, 2020.

Yan, C. Q., Zheng, M., Bosch, C., Andersson, A., Desyaterik, Y., Sullivan, A. P., Collett, J. L., Zhao, B., Wang, S. X., He, K. B., and G., Ö.: Important fossil source contribution to brown carbon in Beijing during winter, Scientific Reports, 7, 43182, https://doi.org/10.1038/srep43182, 2017.

Yan, C. Q., Zheng, M., Sullivan, A. P., Bosch, C., Desyaterik, Y., Andersson, A., Li, X. Y., Guo, X. S., Zhou, T., Gustafsson, O., and Collett, J. L.: Chemical characteristics and light-absorbing property of water-soluble organic carbon in Beijing: Biomass burning contributions, Atmospheric Environment, 121, 4-12, https://doi.org/10.1016/j.atmosenv.2015.05.005, 2015.

Yang, L., Huang, R.-J., Shen, J., Wang, T., Gong, Y., Yuan, W., Liu, Y., Huang, H., You, Q., Huang, D. D., and Huang, C.: New insights into the brown carbon chromophores and formation pathways for aqueous reactions of α-dicarbonyls with amines and ammonium, Environmental Science & Technology, 57, 12351-12361, https://doi.org/10.1021/acs.est.3c04133, 2023.

Yang, X., Huang, S., Li, D., Xu, H., Zeng, Y., Yang, L., Wang, D., Zhang, N., Cao, J., and Shen, Z.: Water-soluble organic matter with various polarities in $PM_{2.5}$ over Xi'an, China: Abundance, functional groups, and light absorption, Particuology, 84, 281-289, https://doi.org/10.1016/j.partic.2023.07.005, 2024.

Yang, Y., Qin, J., Qi, T., Zhou, X., Chen, R., Tan, J., Xiao, K., Ji, D., He, K., and Chen, X.: Fluorescence characteristics of particulate water-soluble organic compounds emitted from coal-fired boilers, Atmospheric Environment, 223, 117297, https://doi.org/10.1016/j.atmosenv.2020.117297, 2020.

You, B., Zhang, Z., Du, A., Li, Y., Sun, J., Li, Z., Chen, C., Zhou, W., Xu, W., Lei, L., Fu, P., Hou, S., Li, P., and Sun, Y.: Seasonal characterization of chemical and optical properties of water-soluble organic aerosol in Beijing, Science of The Total Environment, 930, 172508, https://doi.org/10.1016/j.scitotenv.2024.172508, 2024.

Yu, X., Song, W., Yu, Q., Li, S., Zhu, M., Zhang, Y., Deng, W., Yang, W., Huang, Z., Bi, X., and Wang, X.: Fast screening compositions of $PM_{2.5}$ by ATR-FTIR: Comparison with results from IC andOC/EC analyzers, Journal of Environmental

Sciences, 71, 76-88, https://doi.org/10.1016/j.jes.2017.11.021, 2018.

Yuan, W., Huang, R. J., Yang, L., Guo, J., Chen, Z. Y., Duan, J., Wang, T., Ni, H. Y., Han, Y. M. M., Li, Y. J., Chen, Q., Chen, Y., Hoffmann, T., and O'Dowd, C.: Characterization of the light-absorbing properties, chromophore composition and sources of brown carbon aerosol in Xi'an, northwestern China, Atmospheric Chemistry and Physics, 20, 5129-5144, https://doi.org/10.5194/acp-20-5129-2020, 2020.

Yue, S., Zhu, J., Chen, S., Xie, Q., Li, W., Li, L., Ren, H., Su, S., Li, P., Ma, H., Fan, Y., Cheng, B., Wu, L., Deng, J., Hu, W., Ren, L., Wei, L., Zhao, W., Tian, Y., Pan, X., Sun, Y., Wang, Z., Wu, F., Liu, C.-Q., Su, H., Penner, J. E., Pöschl, U., Andreae, M. O., Cheng, Y., and Fu, P.: Brown carbon from biomass burning imposes strong circum-Arctic warming, One Earth, 5, 293-304, https://doi.org/10.1016/j.oneear.2022.02.006, 2022.

Zellner, R., Exner, M., and Herrmann, H.: Absolute OH quantum yields in the laser photolysis of nitrate, nitrite and dissolved H_2O_2 at 308 and 351 nm in the temperature range 278-353 K, Journal of Atmospheric Chemistry, 10, 411-425, https://doi.org/10.1007/bf00115783, 1990.

Zhang, C., Gao, S., Yan, F., Kang, S., He, C., and Li, C.: An overestimation of light absorption of brown carbon in ambient particles caused by using filters with large pore size, Science of the Total Environment, 833, 155286, https://doi.org/10.1016/j.scitotenv.2022.155286, 2022a.

Zhang, J., Qi, A., Wang, Q., Huang, Q., Yao, S., Li, J., Yu, H., and Yang, L.: Characteristics of water-soluble organic carbon (WSOC) in $PM_{2.5}$ in inland and coastal cities, China, Atmospheric Pollution Research, 13, 101447, https://doi.org/10.1016/j.apr.2022.101447, 2022b.

Zhang, T., Shen, Z., Zeng, Y., Cheng, C., Wang, D., Zhang, Q., Lei, Y., Zhang, Y., Sun, J., Xu, H., Ho, S. S. H., and Cao, J.: Light absorption properties and molecular profiles of HULIS in $PM_{2.5}$ emitted from biomass burning in traditional "Heated Kang" in Northwest China, Science of the Total Environment, 776, 146014, https://doi.org/10.1016/j.scitotenv.2021.146014, 2021.

Zhao, R., Zhang, Q., Xu, X., Wang, W., Zhao, W., Zhang, W., and Zhang, Y.: Light absorption properties and molecular compositions of water-soluble and methanol-soluble organic carbon emitted from wood pyrolysis and combustion, Science of the Total Environment, 809, 151136, https://doi.org/10.1016/j.scitotenv.2021.151136, 2022.

Zhong, M. and Jang, M.: Dynamic light absorption of biomass-burning organic carbon photochemically aged under natural sunlight, Atmospheric Chemistry and Physics, 14, 1517-1525, https://doi.org/10.5194/acp-14-1517-2014, 2014.

Zhong, M., Xu, J., Wang, H., Gao, L., Zhu, H., Zhai, L., Zhang, X., and Zhao, W.: Characterizing water-soluble brown carbon in fine particles in four typical cities in northwestern China during wintertime: integrating optical properties with chemical processes, Atmospheric Chemistry and Physics, 23, 12609-12630, https://doi.org/10.5194/egusphere-2023-752, 2023.

Zhu, C., Cao, J., Huang, R., Shen, Z., Wang, Q., and Zhang, N.: Light absorption properties of brown carbon over the southeastern Tibetan Plateau, Science of The Total Environment, 625, 246-251, https://doi.org/10.1016/j.scitotenv.2017.12.183, 2018.

https://doi.org/10.5194/egusphere-2024-2416
Preprint. Discussion started: 20 August 2024

Tables and Figures

Table 1. Light absorption and fluorescence parameters of WSOC measured in this study.

Sites	Regions	Abs_{365} (Mm^{-1})	MAE_{365} ($m^2 \cdot g^{-1}$)	$AAE_{330-400}$	FI	BIX	HIX
		Avg ± SD	Avg ± SD	Avg ± SD	Avg ± SD	Avg ± SD	Avg ± SD
Tianjin	North China	5.57 ± 3.83	0.89 ± 0.22	6.54 ± 0.64	1.48 ± 0.06	0.97 ± 0.06	2.91 ± 0.37
Handan		13.07 ± 6.95	1.26 ± 0.34	5.59 ± 0.28	1.55 ± 0.08	1.00 ± 0.11	1.07 ± 0.43
Qingdao	East China	4.80 ± 3.09	1.03 ± 0.34	9.17 ± 0.88	1.58 ± 0.09	1.08 ± 0.11	1.69 ± 0.32
Nanjing		6.26 ± 3.26	0.89 ± 0.25	6.08 ± 0.38	1.49 ± 0.17	0.82 ± 0.12	0.56 ± 0.20
Shanghai		1.12 ± 0.53	0.56 ± 0.11	6.61 ± 0.68	1.57 ± 0.09	1.02 ± 0.08	1.98 ± 0.26
Xi'an	Northwest China	10.59 ± 4.42	1.04 ± 0.11	4.07 ± 1.42	1.58 ± 0.08	0.96 ± 0.09	1.53 ± 0.33
Chengdu	Southwest China	5.99 ± 2.61	0.65 ± 0.11	6.29 ± 0.41	1.54 ± 0.10	0.80 ± 0.07	1.18 ± 0.25
Chongqing		10.56 ± 4.10	0.98 ± 0.09	5.62 ± 0.36	1.51 ± 0.04	0.84 ± 0.04	1.37 ± 0.24
Mt. Tai	Regional site	2.66 ± 1.22	0.74 ± 0.24	6.93 ± 0.50	1.31 ± 0.17	0.75 ± 0.15	0.26 ± 0.11
Heshan		3.76 ± 1.55	0.64 ± 0.12	6.06 ± 0.35	1.49 ± 0.03	0.77 ± 0.06	0.91 ± 0.15

https://doi.org/10.5194/egusphere-2024-2416
Preprint. Discussion started: 20 August 2024

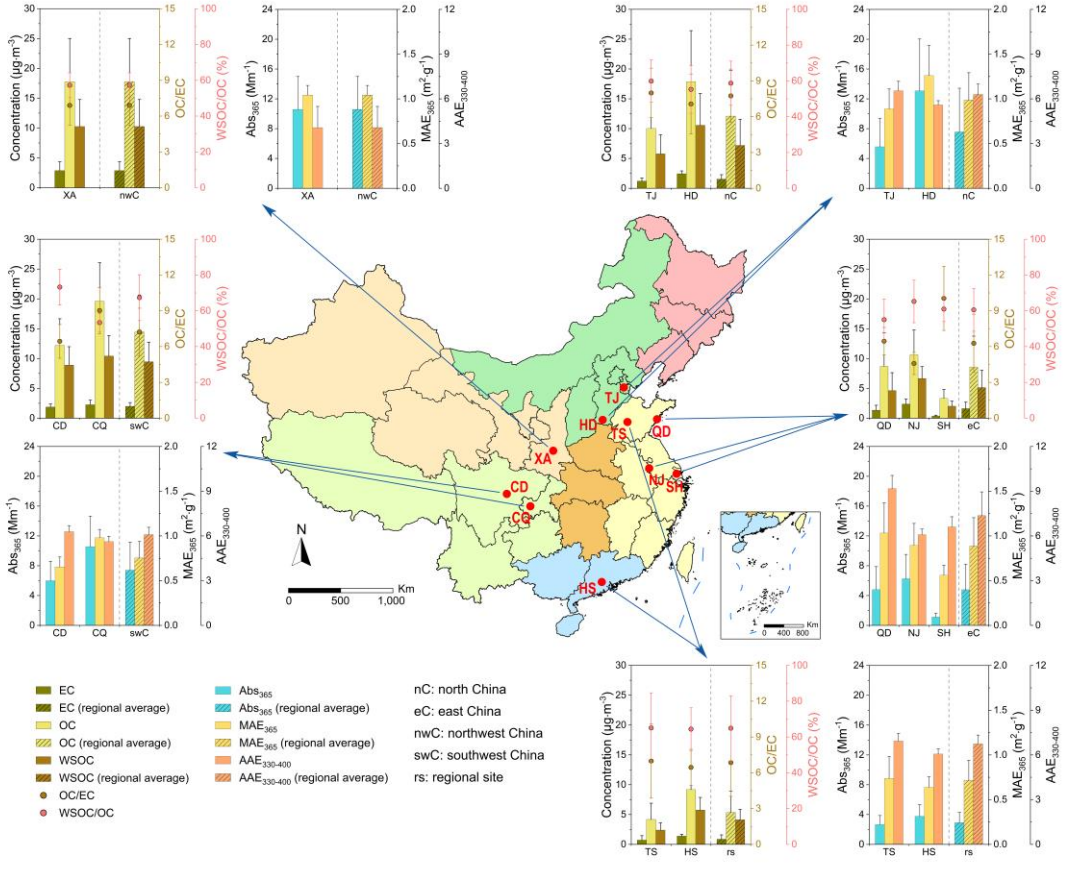

Figure 1. Location map of ten sampling sites and mass concentrations of carbonaceous components (OC, EC and WSOC), OC/EC and WSOC/OC ratios, and light absorption coefficients and mass absorption efficiencies at 365 nm, as well as absorption Ångström exponent at 330-400 nm of WSOC at each site. Note: Data used in the figure are all average values, with shaded columns representing the average value of each region (nwC: northwest China; nC: north China; swC: southwest China; eC: east China; and rs: regional sites) where the sampling sites locate.

https://doi.org/10.5194/egusphere-2024-2416
Preprint. Discussion started: 20 August 2024

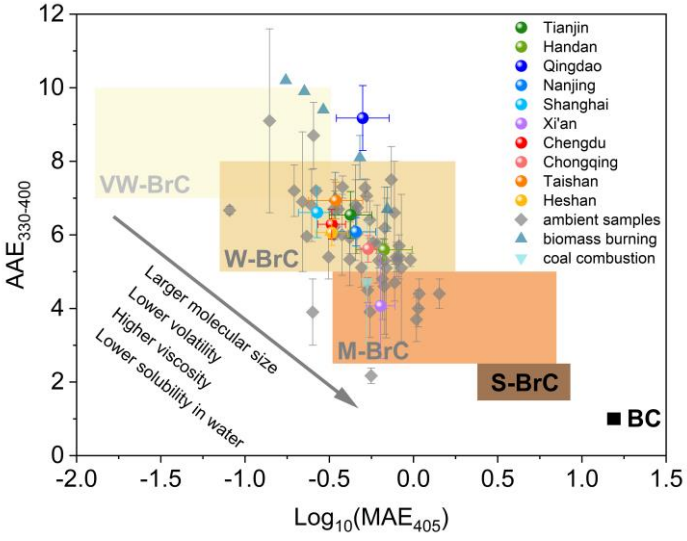

Figure 2. Graphical representation of optical-based BrC classes in log10(MAE_{405})-AAE space. The shaded regions represent very weakly light-absorbing BrC (VW-BrC), weakly light-absorbing BrC (W-BrC), moderately light-absorbing BrC (M-BrC), strongly light-absorbing BrC (S-BrC), and absorbing BC, respectively (Date source: Cheng et al., 2011; Yan et al., 2015; Cheng et al., 2016; Fan et al., 2016; Huang et al., 2018; Yuan et al., 2020; Liu et al., 2018; Chen et al., 2018; Kirillova et al., 2014; Srinivas et al., 2016; Hecobian et al., 2010; Soleimanian et al., 2020; Srinivas and Sarin, 2014; Dey et al., 2021; Zhu et al., 2018; Kirillova et al., 2016; Srinivas and Sarin, 2013; Bosch et al., 2014; Tang et al., 2021; Wu et al., 2020; Liu et al., 2019; Li et al., 2019a; Xu et al., 2020; Yan et al., 2017; Xie et al., 2020; Choudhary et al., 2021; Yue et al., 2022; Deng et al., 2022; Li et al., 2023c; Zhong et al., 2023; Li et al., 2023a; Fang et al., 2023; Ting et al., 2022; Yang et al., 2020; Zhao et al., 2022).

https://doi.org/10.5194/egusphere-2024-2416
Preprint. Discussion started: 20 August 2024

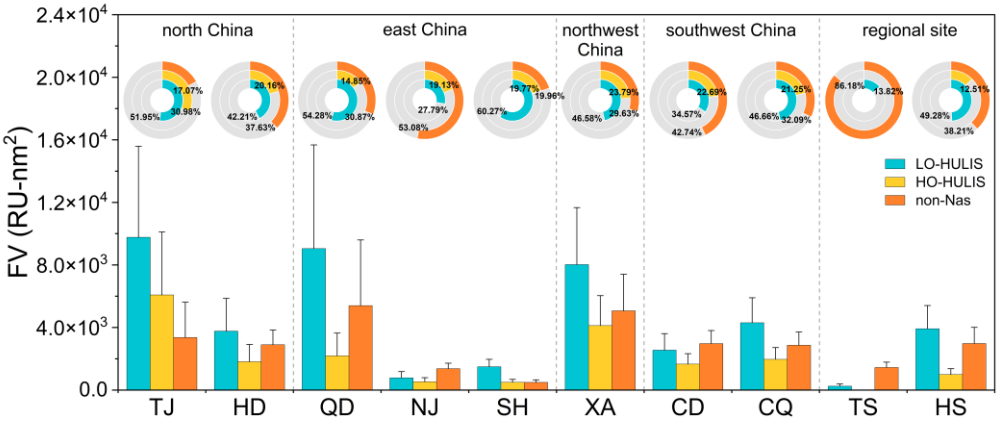

Figure 3. Fluorescence volumes and fractional contributions (circular graph) of various fluorophores at different sites.

https://doi.org/10.5194/egusphere-2024-2416
Preprint. Discussion started: 20 August 2024

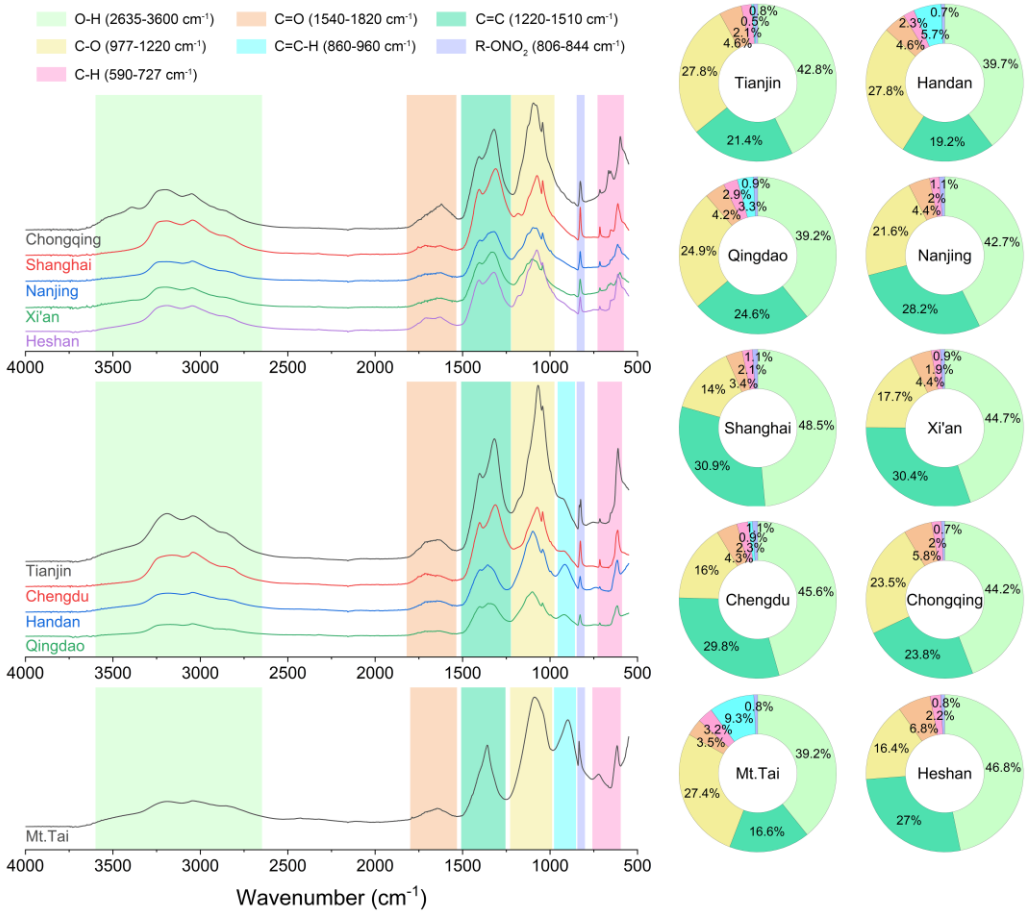

740 **Figure 4.** FTIR spectra of WSOC and relative proportions of different functional groups measured (ring charts) at ten sites in this study.

https://doi.org/10.5194/egusphere-2024-2416
Preprint. Discussion started: 20 August 2024

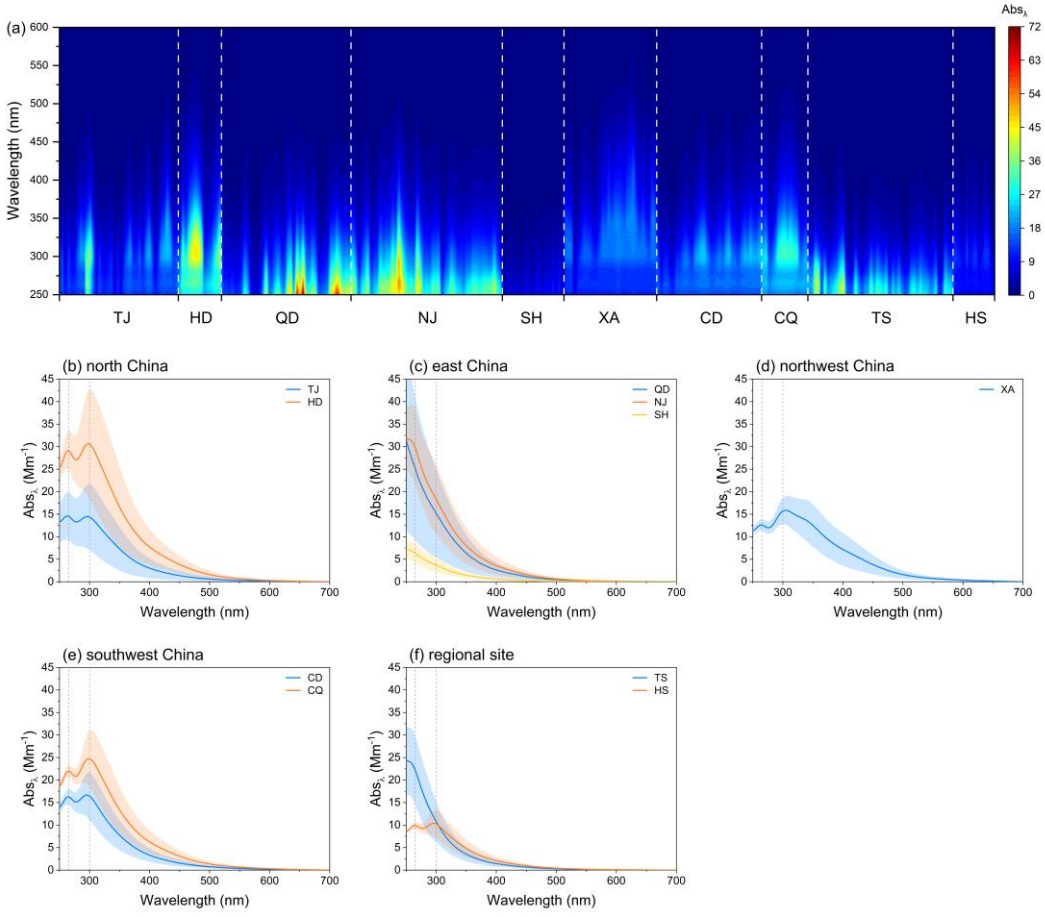

Figure 5. (a) Light absorption coefficient spectrum of WSOC at each site and the average light absorption spectrum in (b) north China, (c) east China, (d) northwest China, (e) southwest China, and (f) regional sites. Note: The color bar represents the magnitude of the Abs_{λ}.

https://doi.org/10.5194/egusphere-2024-2416
Preprint. Discussion started: 20 August 2024

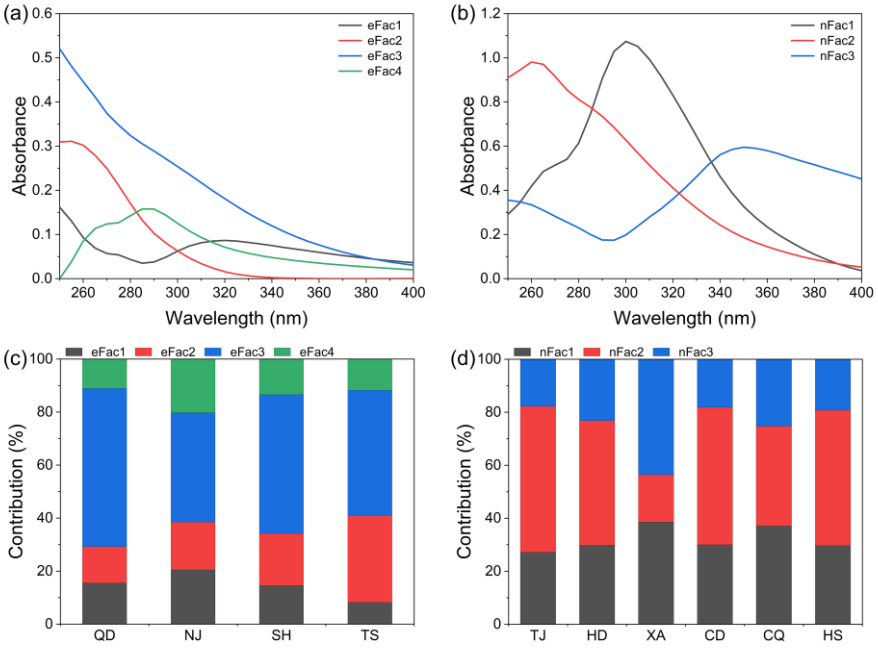

Figure 6. Light absorption spectrum of PMF model resolved factors at (a) east China and (b) outside east China, and average contribution by each factor within the range of 250-400 nm at the (c) east China sites and (d) outside east China sites.

https://doi.org/10.5194/egusphere-2024-2416
Preprint. Discussion started: 20 August 2024

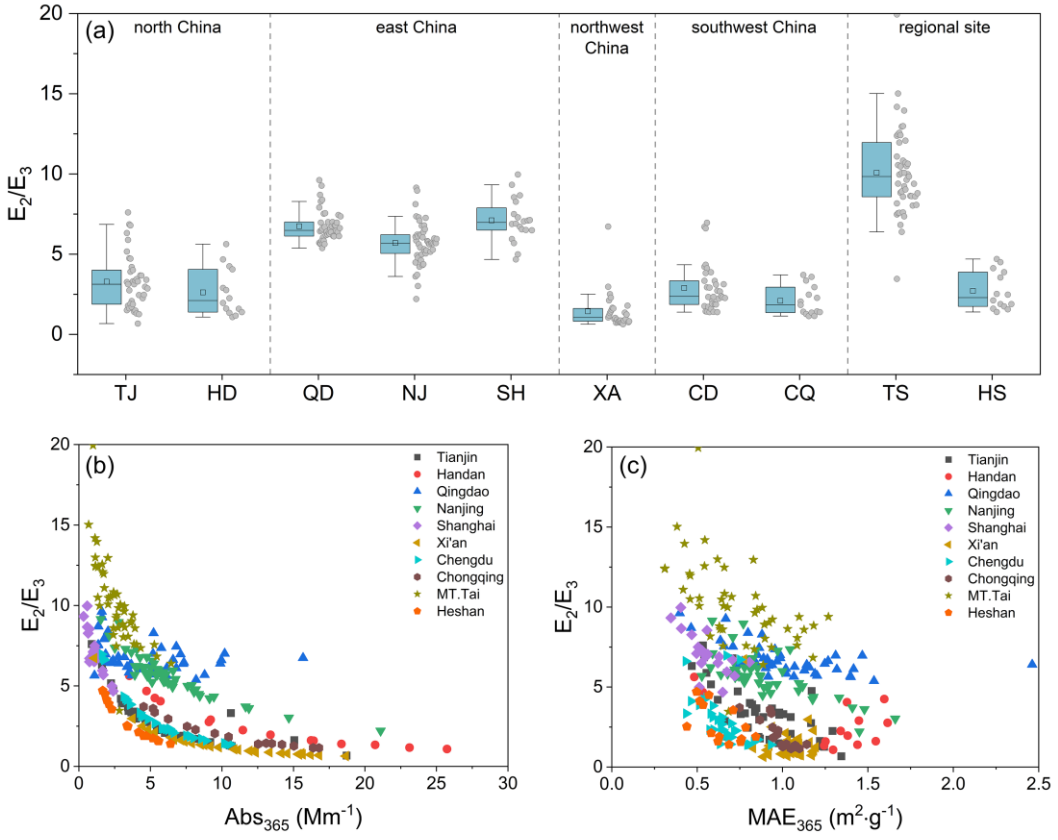

Figure 7. Box-plot of E_2/E_3 at ten sites (Panel a) and scatter plots of relationships between Abs_{365} (MAE_{365}) and E_2/E_3 (Panel b and c).

https://doi.org/10.5194/egusphere-2024-2416
Preprint. Discussion started: 20 August 2024

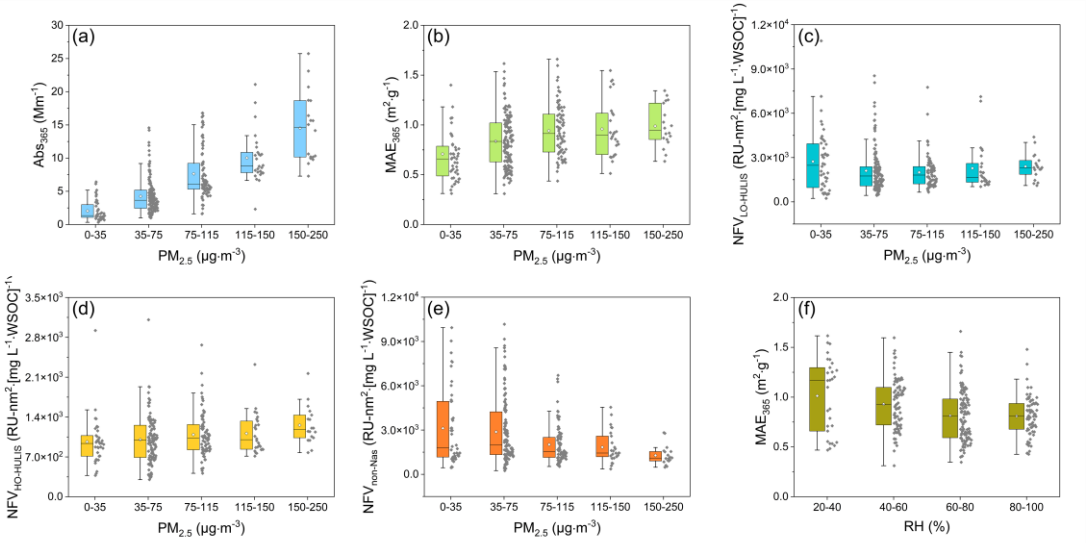

Figure 8. Variations of Abs_{365} and MAE_{365} (Panel a and b), and NFV of different fluorophores (Panel c, d and e) with $PM_{2.5}$ mass concentrations, and MAE_{365} in different RH ranges (Panel f).

https://doi.org/10.5194/egusphere-2024-2416
Preprint. Discussion started: 20 August 2024

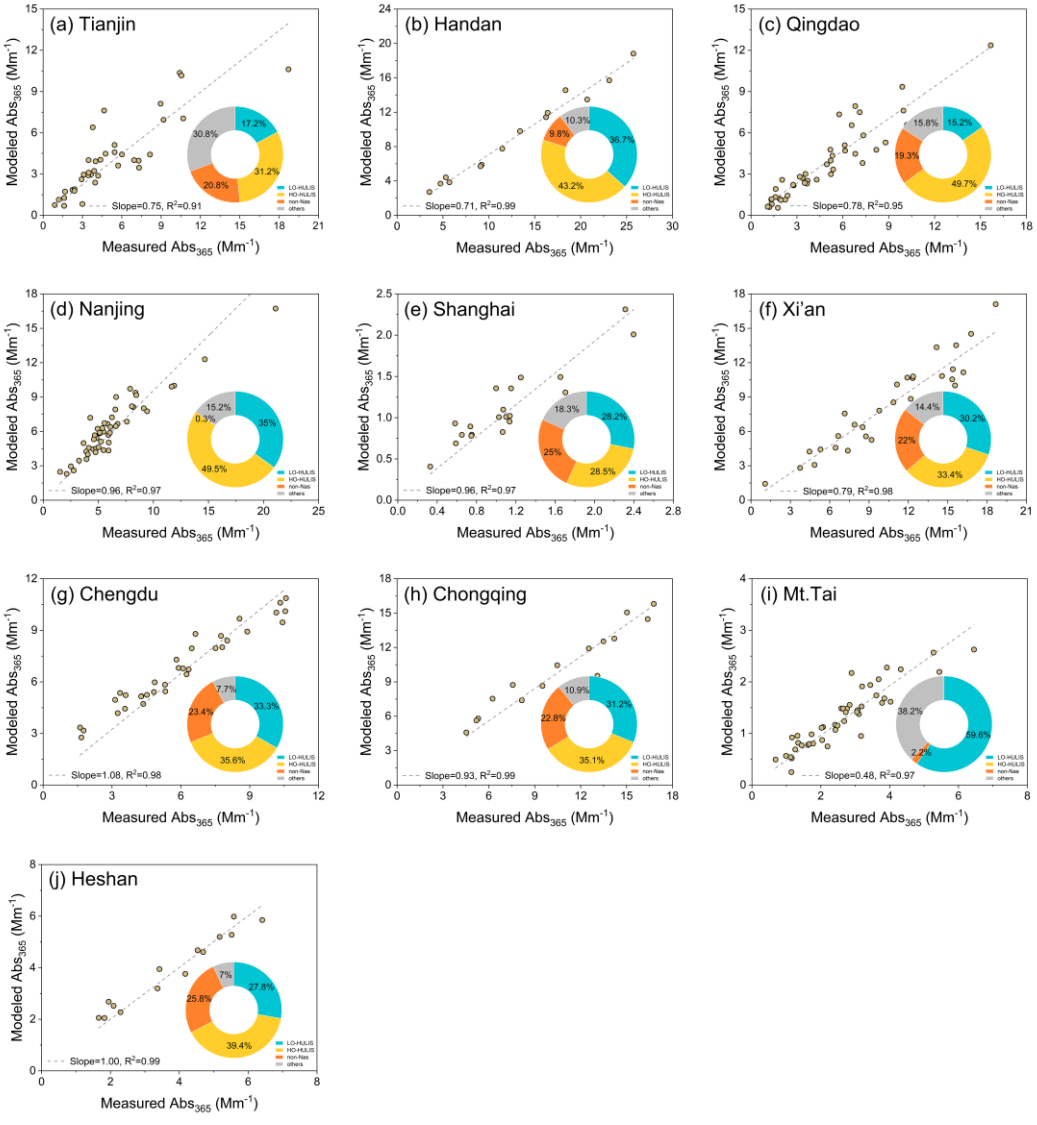

755

Figure 9. Relationships between measured and modeled Abs_{365} based on multiple linear regression (MLR) analysis and fractional contributions of different fluorophores (F_{max}) to total Abs_{365} of WSOC (circular graph) at each site.

https://doi.org/10.5194/egusphere-2024-2416
Preprint. Discussion started: 20 August 2024

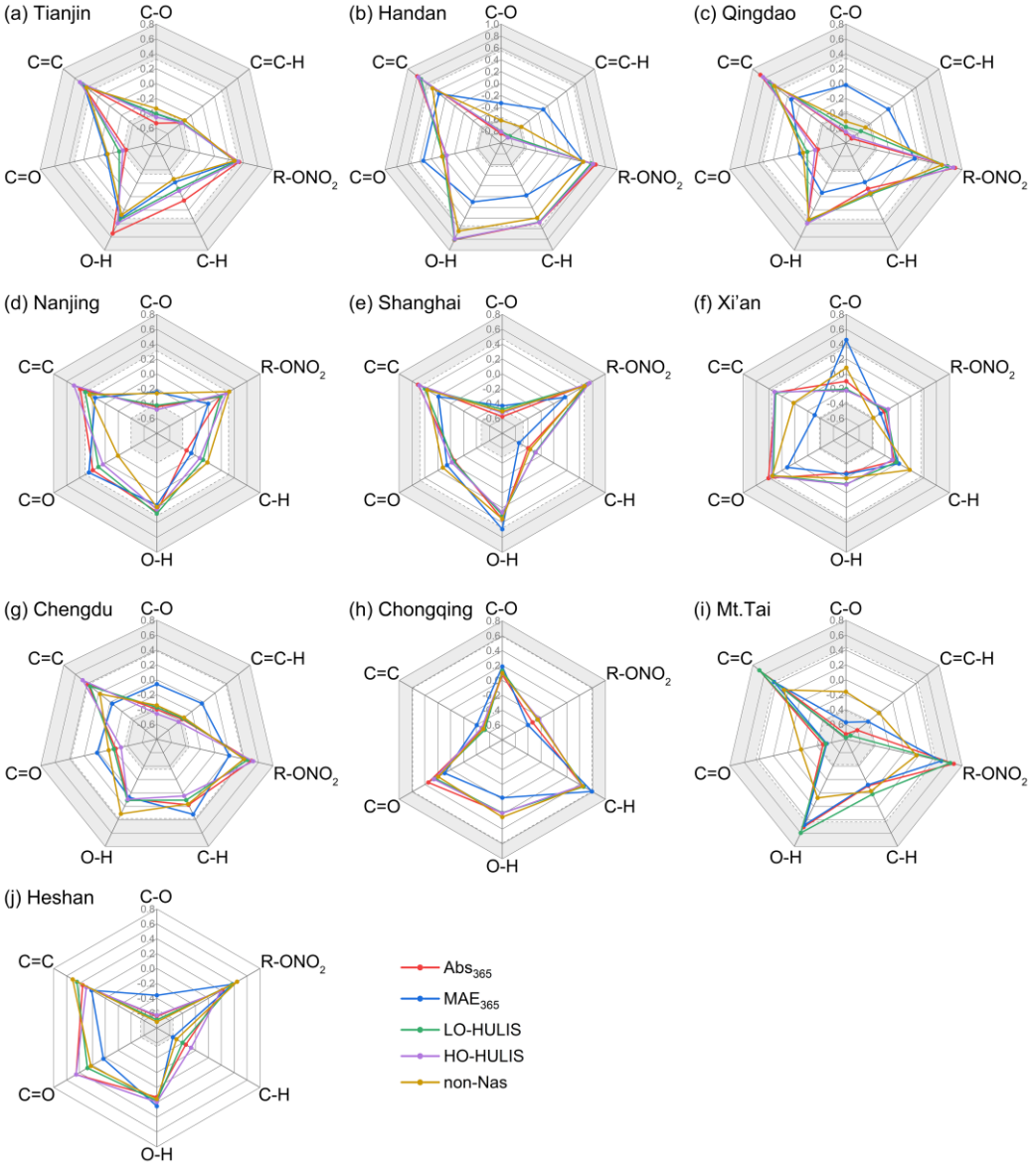

Figure 10. Correlation plots among proportion of functional groups, absorbance parameters (Abs_{365} and MAE_{365}), and F_{max} of fluorophores (LO-HULIS, HO-HULIS and non-Nas). Note: The shaded in the radar chart denote the significantly positive or negative correlation ($p < 0.05$).